

Measures of Disease Activity in Glaucoma

Yue Wu^{1,2}., Maja Szymanska³., Yubing Hu^{2}., Nan Jiang²., Ali K. Yetisen²., M. Francesca*

Cordeiro^{3,4,5}.*

¹Department of Surgery and Cancer, Imperial College London, South Kensington, London, United Kingdom

²Department of Chemical Engineering, Imperial College London, South Kensington, London, United Kingdom

³The Imperial College Ophthalmic Research Group (ICORG), Imperial College London, London, United Kingdom

⁴The Western Eye Hospital, Imperial College Healthcare NHS Trust (ICHNT), London, United Kingdom

⁵Glaucoma and Retinal Neurodegeneration Group, Department of Visual Neuroscience, UCL Institute of Ophthalmology, London, United Kingdom

*Corresponding Author(s): Dr. Yubing Hu: yubing.hu@imperial.ac.uk; Prof. M. Francesca Cordeiro: m.cordeiro@imperial.ac.uk

Abstract Glaucoma is a group of neurodegenerative diseases and a leading cause of irreversible blindness. It significantly affects the quality of life and has a substantial economic impact. Regular eye examinations are important for detecting the disease early and preventing deterioration of vision and quality of life. Current methods of measuring disease activity are powerful in describing the functional and structural changes in glaucomatous eyes. However, there is still a need for a novel tool to detect glaucoma earlier and more accurately. Tear fluid biomarker analyzing and newer imaging technology are able to provide new surrogate endpoints of glaucoma. Artificial intelligence is a post-diagnostic tool can analyse ophthalmic test results. This paper presents a review of currently used clinical tests in glaucoma and highlights the advanced technologies for glaucoma measurement which can identify specific disease characteristics. The mechanism, performance and future perspectives of these devices are introduced. With the development in imaging tools, sensor technologies and artificial intelligence, diagnostic evaluation of this disease must assess more variables to facilitate earlier diagnosis and management decisions in the future.

Keywords Glaucoma, Routine Tests, Glaucoma Biomarkers, Detection of Apoptosing Retinal Cells, Artificial Intelligence

1. Introduction

Glaucoma is a leading cause of irreversible blindness worldwide reason group of ocular neuropathies related to a progressive degeneration of optic nerve and damage to retinal ganglion cells (RGCs)(Davis et al. 2016) (Figure 1). Glaucomatous neurodegeneration results in disconnection in the visual signal between the retina and the brain, subsequently leading to irreversible blindness. It is estimated that around 111.8 million people will be affected by glaucoma by 2040(Tham et al. 2014). Glaucoma often progresses asymptotically and remains undetected until the later stages(Muramatsu et al. 2010). Indeed, as Weinreb et al

discuss, only 10 - 50% of patients are aware of having glaucoma(Weinreb et al. 2014). Moreover, the resultant visual impairment can lead to anxiety and depression contributing to a significant psychological burden(Quaranta et al. 2016).

Aside from the physical and psychological aspects, glaucoma has a substantial economic impact. One study estimated that in 2005 primary open angle glaucoma (POAG) cost the Australian healthcare system 355 million Australian Dollars with costs expected to rise to 784 million by 2025(Dirani et al. 2011). However, the true cost could be higher, as patients often remain asymptomatic and do not seek treatment until the disease is at an advanced stage(Varma et al. 2011). There are few papers suggest the effect is more profound than in the developed world(Lazcano-Gomez et al. 2016). This is compounded by the fact that as the disease progresses it gets more expensive to manage(Varma et al. 2011) (Traverso et al. 2005). A study showed that the direct costs of suspected or early glaucoma (stage 0) were around 623 US Dollars per person per year. For stages one to five, the costs increased to 1480, 1765, 1915, 2464 and 2511 US Dollars per person per year, respectively(Lee et al. 2006). Considering this, early detection of glaucoma should be a priority to prevent the progression of disease, safeguard a patient's wellbeing and reduce personal and national expenditure.

Current methods of identifying glaucoma include intraocular pressure (IOP) measurements, visual field (VF) testing, and optical coherence tomography (OCT) with each technique examining different features of the disease process (Figure 1)(Phu et al. 2020). It is particularly well established that an increase in IOP increases the risk of glaucoma progression. VF testing directly reflects the level of functional damage, and the rate of progression of visual field loss can be used as a predictor of future disease. OCT can assess the retinal nerve fibre layer(RNFL) and the rate of loss of RNFL can be used in predicting progression – 18 months before visual field(Harasymowycz et al. 2016; Phu et al. 2020; Yap et al. 2020a) (Wu and Medeiros 2018). Despite these methods, there is still a lack of agreement among glaucoma specialists due to

lack of consistent and quantitative clinical criteria(Phu et al. 2020). Therefore, research is ongoing to develop diagnostic tools that are more specific and can detect glaucoma earlier. Tear fluid analysis and Detection of Apoptosing Retinal Cells (DARC) are currently in development(Cordeiro et al. 2021). Both of these methods rely on different features of the disease process to estimate the risk of glaucoma. Besides, Artificial Intelligence (AI) has a great potential to help analyse functional and structural parameters of eyes(Devalla et al. 2020)

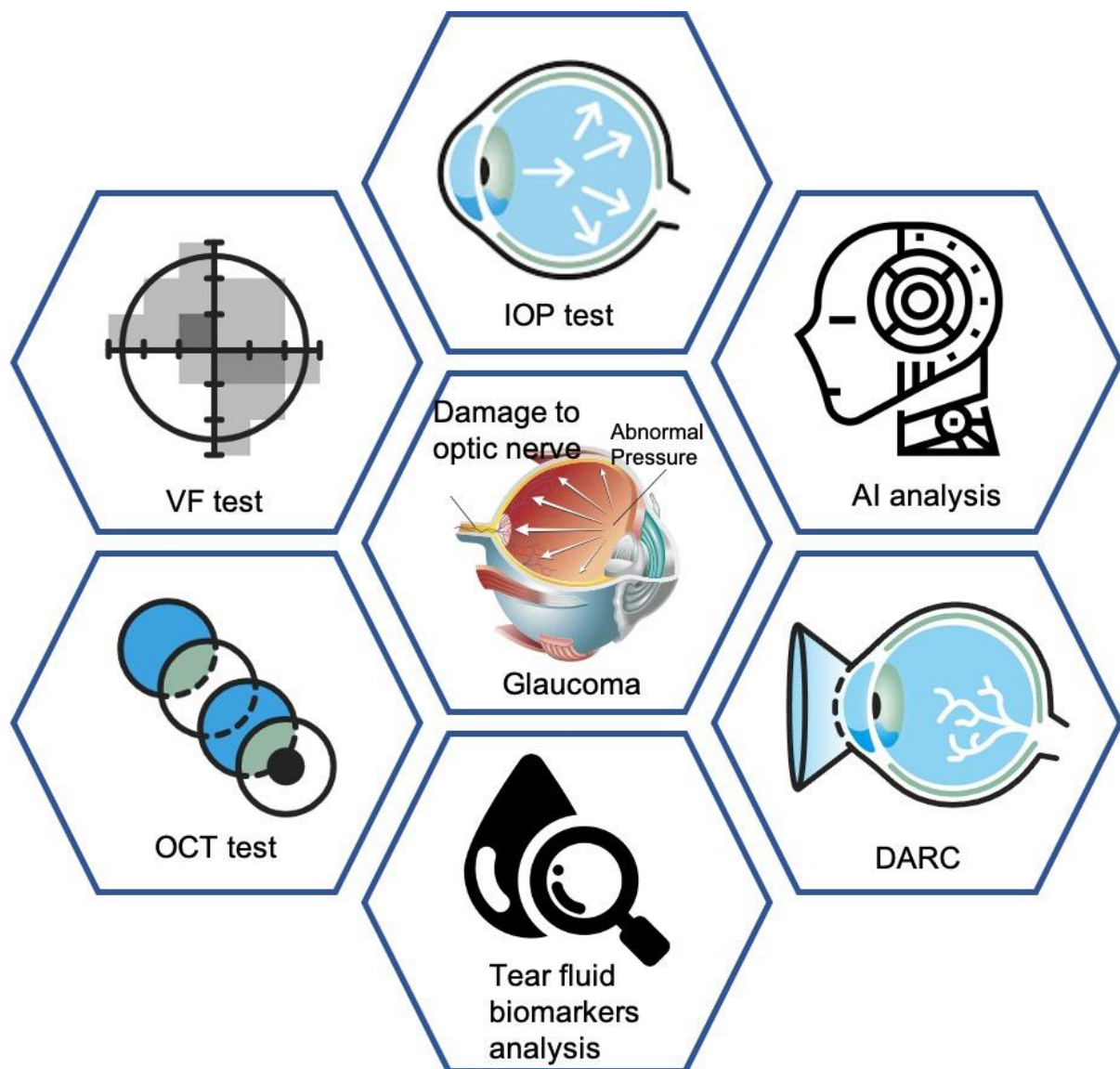


Figure 1. Schematic illustrations of diagnostic tool of glaucoma. Traditionally, methods of identifying glaucoma IOP measurements, VF testing, and OCT. Tear fluid analysis and DARC

have great potential to detect glaucoma progression with high accuracy. AI provides a novel platform to analyse the results of clinical tests.

This review aims to discuss the clinical measures of activity in glaucoma and their current use in research and clinical practice. It summarises the current techniques for the measurement of glaucoma disease activity, including IOP testing, VF testing and OCT. Furthermore, several promising methods in development are discussed, including tear molecular biomarkers analysis, DARC, genetic testing and AI. These techniques help us assess different features of the disease process, including molecular change, neurodegeneration, and genetic abnormality which may help identify the disease at an early stage and guide treatment.

2. Current clinical measurements of glaucoma

At present, a diagnosis of glaucoma is based on several measures of disease activity including clinical history, IOP measurement, VF testing and OCT images(Harasymowycz et al. 2016). Measurement of IOP plays an important role in determining the diagnosis(Schuster et al. 2020). VF testing is a powerful tool to estimate functional loss of vision. OCT is useful for identifying glaucomatous changes in the back of eye and can provide objective measurement of the retinal nerve fibre layer (RNFL), optic nerve head (ONH) and macula, which all can indicate the severity of glaucoma(Jampel et al. 2009).

2.1 Intraocular Pressure Test

IOP is a measurement of the fluid pressure within the eye and is maintained through a balance of aqueous humour production and outflow(Acott et al. 2014; Costagliola et al. 2020). Several clinical trials demonstrating that even a small increase in IOP can affect the visual function(Jayanetti et al. 2020; Nuyen and Mansouri 2015). Considering this, measures the IOP precisely plays an important part in managing glaucoma.

2.1.1 Goldmann Applanation Tonometry

Goldmann applanation tonometry (GAT) is one of the most widely used devices to measure IOP(Chen et al. 2019). The measurement of IOP follows the Imbert-Fick law. The eyeball can be regarded as a sphere filled with liquid and surrounded by a wall. The pressure inside therefore equal to the counter pressure which flattens the membrane(Castro et al. 2016). Thus, the estimation of the IOP follows the equation:

$$IOP \text{ estimation} = F/A. \quad (\text{Eq. 1})$$

F represents the force required to flatten a certain area of the cornea and A is the size of the flattened area(Nuyen and Mansouri 2015). The GAT is attached to a slit lamp (Figure 2a). Patients must be topically anesthetized before the test and a fluorescein dye applied to visualise the patients' tear film. A prism (Figure 2b) attached to a tonometer head is used to produce an applanating force to flatten the centre of the cornea with the size of 7.35 mm² (Kim et al. 2017a) (Figure 1c).

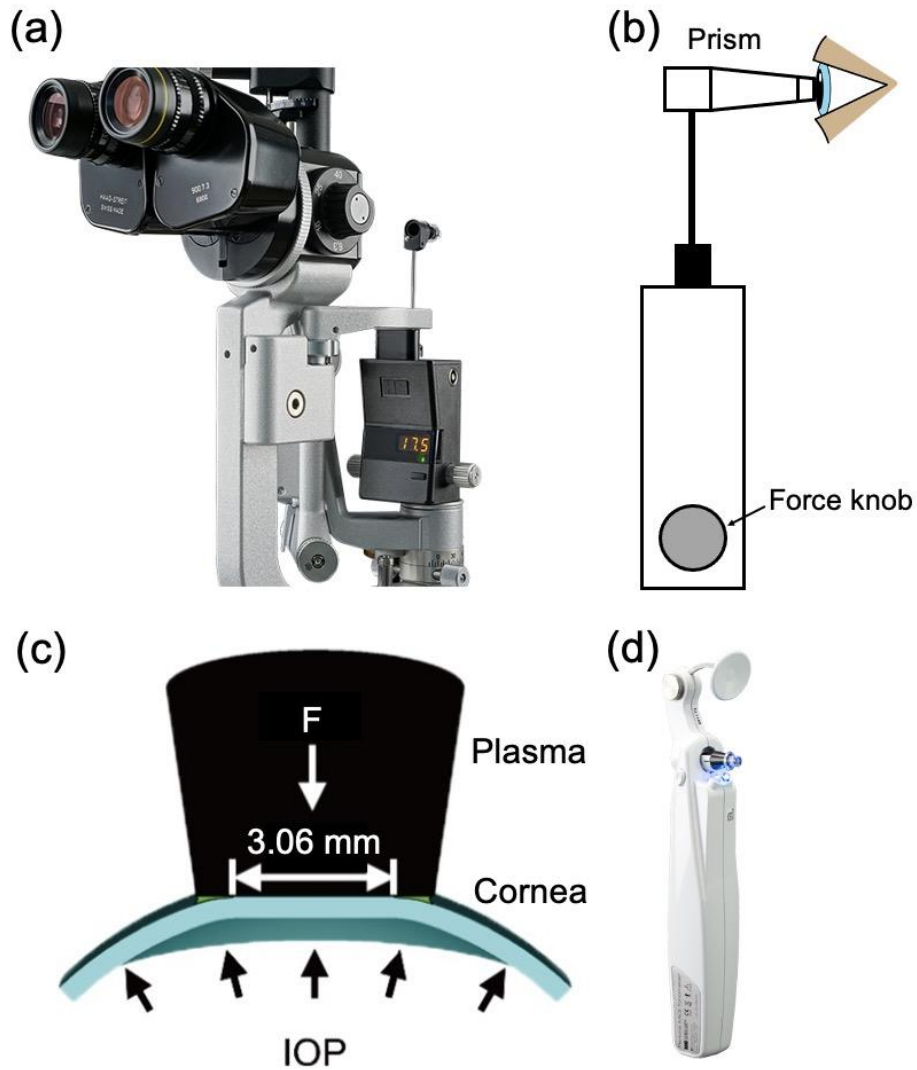


Figure 2. Goldmann Applanation Tonometry a. GAT mounted on a slit lamp. Adapted with permission from Haag-Streit Diagnostics. Copyright ©HAAG-STREIT AG, 3098 Koeniz, Switzerland 4. Edition / 2020 – 02.b. Diagram of GAT. c. Diagram of IOP reading, the tonometer head flattens the area of the cornea (size: 7.35 mm², diameter 3.06 mm). F represent the force applied to applanate the cornea. Adapted with permission from (Kim et al. 2017a). Copyright © 2017 Kim et al. d. A Perkins handheld tonometer. Adapted with permission from Haag-Streit Diagnostics. Copyright ©HAAG-STREIT UK 2020.

GAT shows great validity, reliability, and reproducibility in clinical practice, therefore it is regarded as the gold standard for IOP measurement (Table 1)(Chen et al. 2019). A population-

based study showed that GAT has both low inter and intra-observer variability. In this study, 40 patients were included in inter-observer variability (the difference between multiple measurements taken by different examiners) experiments. The IOP was tested in both left and right eye three times by one clinician. After 10 minutes, the test was repeated by another clinician. The mean difference between the first measurements was 1.79 mmHg with the standard deviation (SD) 2.41 mmHg and the mean difference between the median value of three measurements was 1.60 (SD 2.15) mmHg(Dielemans et al. 1994). Researchers also explored intra-observer variability (the difference between measurements taken by the same examiner) by recruiting 22 patients and measuring the IOP of each eye by the same clinician. The mean difference between the first and median measurements was 1.64 (SD 2.07) mmHg and 1.50 (SD 1.96) mmHg(Dielemans et al. 1994), respectively. This demonstrates that GAT results are reliable when obtained by an appropriately trained clinician.

Despite its strengths GAT is not without its limitations. Corneal biomechanics such as central corneal thickness (CCT) can influence the results obtained with GAT. A raised CCT can result in artificially higher IOP measurements with GAT (Gelaw 2012; McCann et al. 2020). A study demonstrated that the most correct reading was obtained in an eye with CCT of about 520 μ m, and every 100 μ m resulted in 7 mmHg error(Sng et al. 2017). Furthermore, corneal irregularities, such as a flat cornea, conical corneal shape and corneal surgery significantly influence the accuracy of GAT measurement(Ceruti et al. 2009; Nuyen and Mansouri 2015; Papastergiou et al. 2008). Other limitations to be considered during the measuring process include inaccurate usage of fluorescein dye or topical anaesthetics and application of inappropriate pressure directly to the cornea surface. A further limitation of GAT is that it must be mounted on a slit lamp, which may not be suitable for children, elderly, or those with disabilities(Aziz and Friedman 2018; Nuyen and Mansouri 2015; Stamper 2011).

Perkins Handheld Tonometer (Figure 2d) is an alternative device used for IOP measurement which follows a similar principle to GAT(ElMallah and Asrani 2008). It does not require a slit lamp, making it more suitable for patients unable to sit upright. PHT has similar advantages and disadvantages to GAT(ElMallah and Asrani 2008). A study comparing Perkins Handheld Tonometer and GAT by obtaining IOP measurement from 100 eyes found that the difference between reading from these two methods was only 0.22 (SD 0.44) mmHg ($P < 0.001$)(Table 1). The Perkins Handheld Tonometer yielded similar readings to GAT demonstrating that it can be useful in clinical practice especially in patients unable to sit at the slit lamp(Arora et al. 2014).

2.1.2 Non-Contact Tonometry

Non-contact Tonometry is an applanation tonometry and follow the similar principle as GAT to measure IOP. It use a pulse of air to applanate the cornea rather than the prism(Chen et al. 2019), which significantly reduced the risk of infection(Nuyen and Mansouri 2015). A low intensity beam is generated by the light emitter and reflected by the cornea into the detector at the opposite side(Figure 3a). A pulse of air is blown onto the cornea at increasing pressures until the system detects that the cornea is flattened. The pressure of air required to applanate the cornea is used as an analogue of IOP (Jedzierska and Koprowski 2019). The Ocular Response Analyser (ORA) and the Corvis ST are modern examples of the non-contact tonometry (Esporcatte et al. 2020).

ORA can provide a Goldmann-like IOP and a Corneal-Compensated IOP (IOP_{cc}) by using an algorithm to correct for errors introduced by structural factors such as corneal thickness (Kilavuzoglu et al. 2019). A study compared the IOP_{cc} assessed by ORA with the IOP reading of GAT in 94 healthy subjects. The mean value of mean IOP_{cc} was 15.6 ± 3.3 mmHg and Mean GAT-IOP was 12.9 ± 2.4 mmHg indicating that IOP_{cc} overestimated GAT-IOP ($p < 0.001$)(Table 1)(Ramm et al. 2019). However, it is thought that this difference is caused by the

biomechanical correction and that overall GAT-IOP and IOPcc measurements remain consistent with each other (Ramm et al. 2019). In addition to measuring IOP, ORA can also provide a special parameter known as Corneal Hysteresis (CH) (Okafor and Brandt 2015). During the measuring process, the force of the air pulse continues to increase despite the cornea being flattened until a slight indentation is formed. The force then decreases, and the cornea flattens again. This results in two IOP values and the difference is referred to as CH (Figure 3b) (Fujishiro et al. 2020). Evidence shows that the CH is lower in POAG compared with controls (Sayah et al. 2020). However, ORA is a non-portable device, and so may not be suitable for some patients.

Corvis ST can not only provide the IOP reading but can also record the cornea reaction during the measurement. An ultra-high-speed Scheimpflug camera replaces the light system and allows a detailed analysis of corneal movement and calculation of the IOP (Wang et al. 2021). The Corvis ST is able to reduce the biomechanical effect on the IOP measurement by specific algorithm and provides biomechanically corrected IOP (bIOP) (Vinciguerra et al. 2020). Elias et al used a fixed pressure transducer to detect the “true” IOP of 5 cadaver eyes in an ex-vivo environment and found the bIOP was very close to the true IOP (Elias et al. 2018). Another in-vivo study compared the bIOP with GAT-IOP amongst patients with glaucoma and healthy individuals. In all groups, bIOP was significantly lower than GAT-IOP (Vinciguerra et al. 2020). Sedaghat et al found that the bIOP had a less association with corneal thickness (Sedaghat et al. 2019), which permits greater accuracy in measuring IOP.

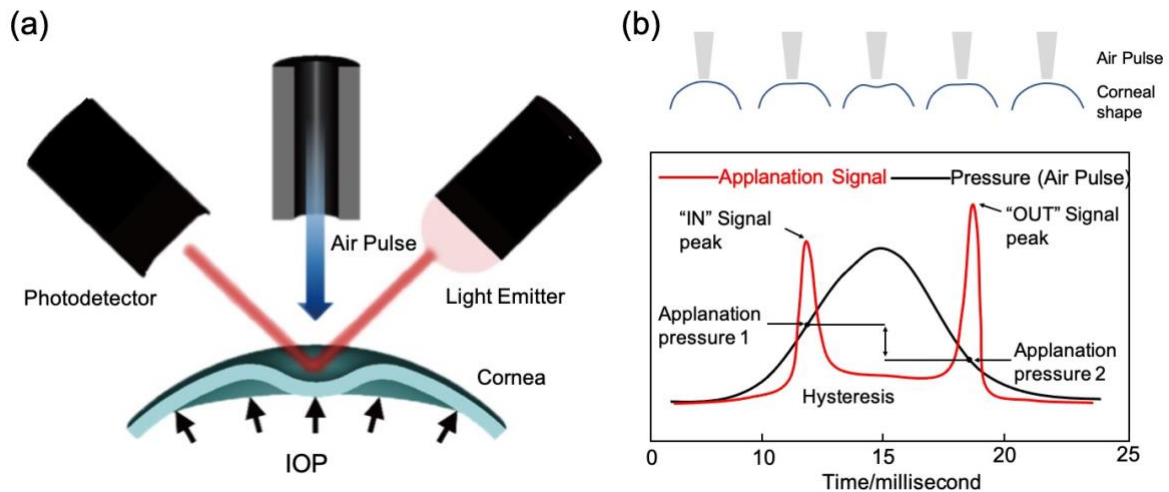


Figure 3. Principle of Non-Contact Tonometry (NCT). a. The air pulse is used to flatten the cornea. A light emitter and a photodetector are located at different sides of eye to detect the flattening of the cornea. Adapted with permission from (Kim et al. 2017a). Copyright © 2017 Kim et al. b. Hysteresis explanation diagram. The force of air steadily increases. When the cornea is flattened, the force is recorded and keeps increasing until a slight indentation form. The force then decreases and there is another applanation point, and the force is recorded again. The difference between these two readings is the corneal hysteresis.

2.1.3 Other common tonometers

The iCare Rebound Tonometer (iCare) uses a magnetised probe that accelerates upon being propelled towards the cornea. When it hits the cornea, it decelerates. In high IOP, the deceleration of the probe is rapid, and it rebounds quicker. When the IOP is low the rebound takes longer due to slower deceleration. The IOP is calculated according to the speed of deceleration and the time of probe rebound (Liu et al. 2020). Subramaniam et al found that the iCare significantly underestimated the GAT IOP by 4.1 mmHg (12.1 mmHg vs 16.2 mmHg) (Table 1)($p < 0.0001$) (Subramaniam et al. 2020). Due to the high speed of the probe and short-lived contact with the cornea, iCare does not require topical anaesthesia making it particularly useful in young children(Uzlu et al. 2020). Additionally, iCare is a relatively straightforward

device that patients can even be trained to test the IOP by themselves(Tan et al. 2017). However, it should be noted that iCare is more susceptible to corneal biomechanical properties than GAT (Gao et al. 2017; Zakrzewska et al. 2019).

To mitigate the effect of corneal biomechanics on IOP readings, a dynamic contour tonometer (DCT) was developed(Nuyen and Mansouri 2015). DCT measure the IOP by tightly attaching to the cornea and applying a hydrostatic pressure to part of the cornea. When this part of the cornea becomes relaxed, the hydrostatic pressure is equal to the IOP(Fuest et al. 2017). As the cornea is not deformed during the measurement, DCT is less affected by corneal biomechanics (Katsimpris et al. 2015; Olyntho Junior et al. 2020). However, the DCT tip needs to be in direct contact with the cornea for 5 seconds to obtain repeated measurements which patients may not be able to tolerate. A study showed the DCT reading was significantly higher than the GAT reading in both glaucoma patients normal people, with differences of 2.19 ± 2.24 mmHg and 2.56 ± 1.94 mmHg ($p < 0.01$) respectively(Table 1)(Yildiz and Yasar 2018). Moreover, DCT is a slit lamp mounted device and requires an appropriately trained clinician. Despite this, DCT shows promise as a tonometer unencumbered by the biomechanical influence of the cornea.

Table 1. Summary of current devices for IOP testing.

Device	Mean difference of IOP measurement compare with GAT (mmHg)	Advantages	Limitations	Reference
Goldmann Applanation Tonometry	-	Low inter and intra-observer variability. Gold standard for IOP measurement.	Affected by Corneal biomechanics. Fluorescein dye and topical anaesthetics required. Non-portable.	Dielemans et al., 1994; Chen et al. 2019;
Perkins Handheld Tonometer	0.22 ± 0.44 , $P < 0.001$	Low inter and intra-observer variability. Portable.	Affected by Corneal biomechanics. Fluorescein dye and topical anaesthetics required.	EIMallah and Asrani 2008; Arora et al. 2014

Non-contact Tonometry	$2.7 \pm 3, P < 0.001$	Less risk of infection. Less affected by structural factors. Provide parameters about corneal structure.	Non-portable	Ramm et al., 2019; Nuyen and Mansouri 2015; Kilavuzoglu et al. 2019
iCare rebound tonometer	$-0.22 \pm 3.07, P = 0.19$	No requirement for topical anaesthesia and fluorescein dye. Portable Patients can be trained to test IOP by themselves.	More susceptible to corneal biomechanical properties. Underestimate the GAT IOP.	Gao et al. 2017; Zakrzewska et al. 2019; Subramaniam et al. 2020
Dynamic contour tonometer	Glaucoma: $2.19 \pm 2.24, P < 0.01$ Normal: $2.56 \pm 1.94, P < 0.01$	Less affected by corneal biomechanics	The test process may not be tolerated by some patients. IOP reading higher than GAT. Non-portable.	Katsimpris et al. 2015; Olyntho Junior et al. 2020; Yildiz and Yasar 2018

2.2 Visual Field Test

The term visual field refers to the entire area that can be seen when the eye looks forward in a fixed direction (Figure 4a)(Phu et al. 2017). A blind spot is a particular area of reduced or total absence of vision located temporally between 10 and 20 degrees (black spot in Figure 3a). VF loss is one of the most common characteristics of glaucoma(Casson et al. 2012). Early and effective intervention can help to slow down the disease progression (Figure 4b) (De Moraes et al. 2017). This highlights the importance of accurate detection and measurement of VF progression in glaucoma patients.

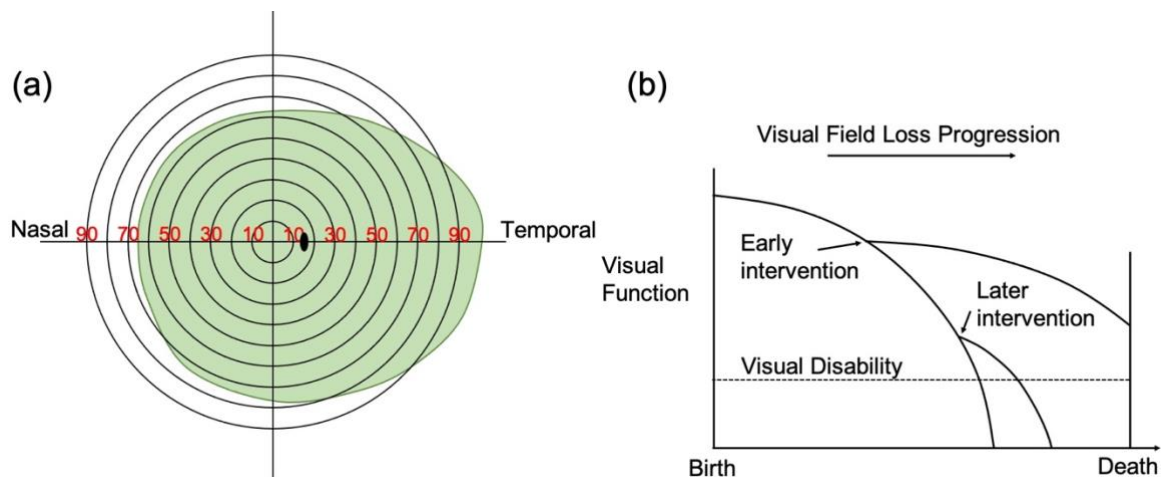


Figure 4. Normal visual field and the effect of ophthalmic intervention on the visual field loss progression at different times. a. the normal visual field extends 50 degrees superiorly, 70 degrees inferiorly, 60 degrees nasally and 100 degrees temporally. The blind spot (black spot) is located between 10 and 20 degrees. b. Intervention started at different time points results in different outcomes. Early intervention significantly slows down the drop in visual function.

2.2.1 Humphrey field analyser (HFA)

The HFA is the most widely used perimetry (Alencar and Medeiros 2011; Camp and Weinreb 2017). A series of achromatic (white) light stimuli of fixed size (Goldmann size III, GIII) but differing intensities (varies from 0 to 51 dB, 0 dB being the brightest stimuli) (Nouri-Mahdavi 2014) are projected from a large, white bowl. Patients are instructed to press the hand-held button when they see the stimulus. Automated algorithms such as Swedish Interactive Thresholding Algorithm (SITA) are used to calculate the patients' capability to recognise the light stimulus at varying intensities and finally locate the damaged area of patient's visual field (De Moraes et al. 2017). Up to now, SITA fast and SITA Faster were developed to further shorten the detection time without influencing the accuracy and reliability of the data (Heijl et al. 2019).

There are several test protocols, including 10-2, 24-2 and 30-2 which detect different area of the visual field. For example, 24-2 means measuring 24 degrees temporally and 30 degrees nasally (Nouri-Mahdavi 2014). The second number 2 indicate the pattern of the points tested. It is crucial to select the appropriate protocol best suited to the patient's condition. For glaucoma monitoring, 24-2 testing model is the most widely accepted pattern due to smaller variability and being faster than other pattern (Wang and Henson 2013). The 10-2 pattern provides a more detailed test of the central area than the 24-2 pattern (Park et al. 2013) (Garg et al. 2018). Although it is known that visual field damage usually starts at the peripheries and central vision tends to be spared until later stages of the disease (Sugisaki et al. 2020). Some

studies have indicated that glaucomatous changes could be found at the central region in the earlier stages of glaucoma(Hood et al. 2013; Wu et al. 2018). Consequently, 10-2 testing strategy helps to estimate the damage to central vision and can be a beneficial addition to 24-2 test(Tomairek et al. 2020).

Analysing an HFA printout can be challenging. The reliability indices (Figure 5b) of the HFA printout reflects the extent to which the patient's results are reliable. Fixation losses indicate the steadiness of gaze throughout the test. The lower the number of fixation losses, the more reliable the test. False positives occur when a patient reports a stimulus in the absence of the stimulus. High false positives represent glaucomatous visual loss and indicate worse results than the one produced by the report. False negatives are detected when a brighter (9 dB) stimulus appears at the location where the threshold has already been determined but patient had not responded. High false negatives indicate that the visual loss is less than what is reported in the test result. The numerical display (Figure 5c) contains the threshold values of each tested point. Lower numbers mean that the patient can only see brighter light. The grey scale (Figure 5d) represents a graphical form of the numerical display. The darker the shade, the lower the sensitivity.

Total deviation (Figure 5e) is the difference between the threshold obtained by the VF test at each point compared against a corresponding reference value obtained from a healthy general population and corrected for age. It is depicted as a numerical plot and a probability plot. The negative values indicate that the sensitivity is lower than normal, whereas positive indicate a higher sensitivity. The pattern deviation (Figure 5f) is derived from total deviation values. It can correct for common causes of decreased visual sensitivity such as lens opacity. Darker spots indicate that a defect is more likely to be significant.

Glaucoma Hemifield Test (GHT) (Figure 5g) provide the asymmetry of corresponding points above and below the horizontal meridian. Visual field index (VFI) (Figure 5h) reflects the

overall visual field function that 100% represents a perfect age-adjusted visual field. Mean deviation (MD) (Figure 4h) indicates the overall sensitivity of the visual field and it is derived from the total deviation. Normal MD ranges from 0 dB to -2 dB and a negative value is consistent with a field loss. Pattern standard deviation (PSD) (Figure 5h) is a measure of focal loss within the visual field. A higher PSD is better than MD in estimating the glaucomatous damage. An upstroke signal and high-frequency movements decrease the accuracy of the test. A downstroke means that the tracker has lost the view of the pupil either due to blinking or droopy upper eyelid(Aggarwal et al. 2018; Yaqub 2012).

Even though HFA has been regarded as a reliable and accurate measure of visual field loss for a long time, it has its drawbacks. HFA testing is a subjective test, the co-operation and responses of the patient play crucial roles in obtaining a reliable result and requires a high level of understanding from patients(Szatmáry et al. 2002). It is can be difficult to perform HFA in certain groups of patients such as children or the elderly. Additionally, learning effect is another factor influencing the accuracy of the test. Learning effect is a phenomenon where the reliability and VF indexes improve when patients become familiar with the visual field test(Aydin et al. 2015). To minimise the learning effect, at least 3 repetitions may be needed(De Tarso Pierre-Filho et al. 2010).

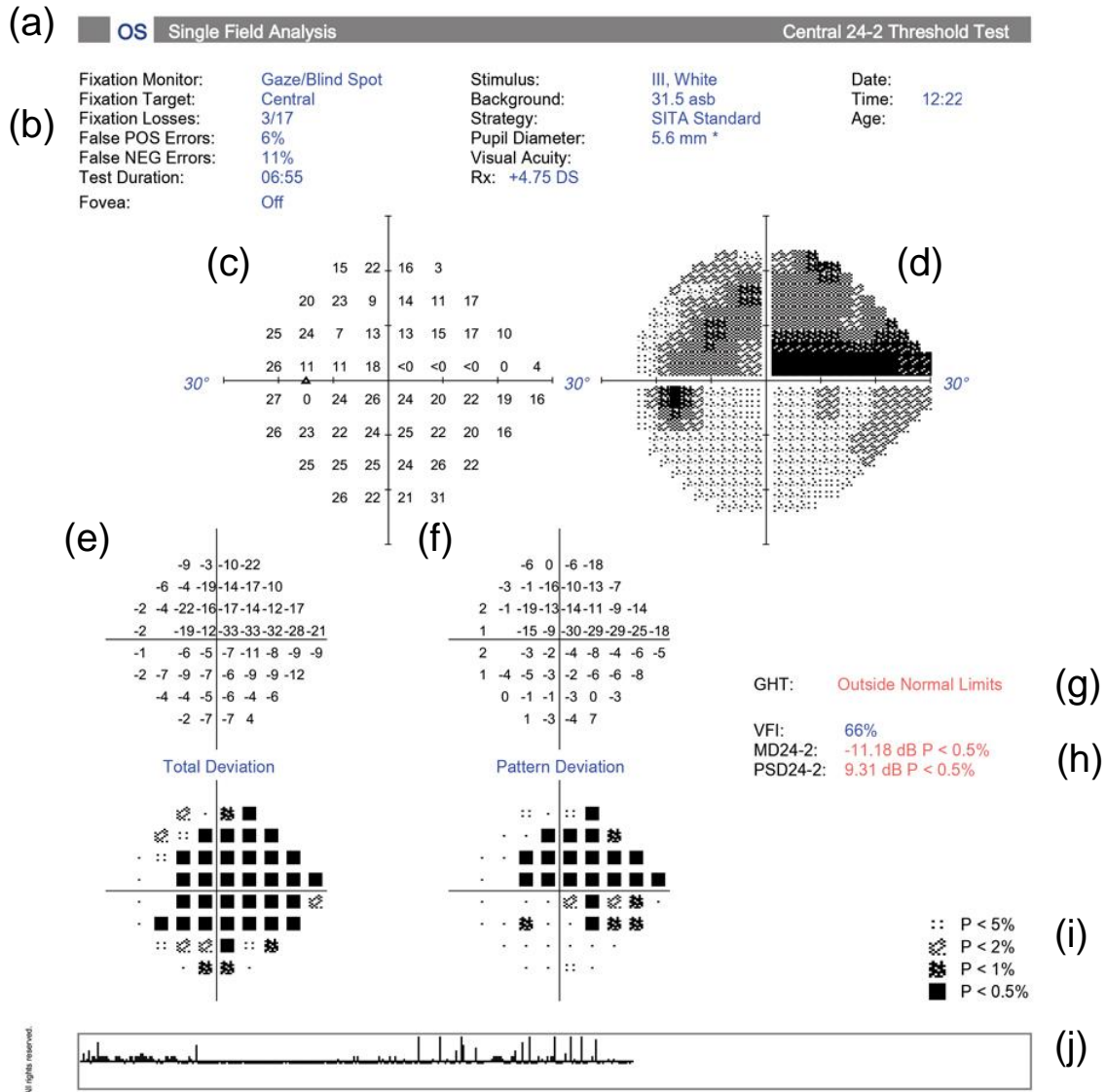


Figure 5. A Humphrey visual field printout. a. Test type; b. Reliability Indices; c. Numeric (dB) Results; d. Grayscale Results; e&f. Deviation Plots; g. Glaucoma Hemifield Test (GHT); h. Global Indices; i. Probability Symbols; j. Gaze tracker. Image Courtesy of ZEISS.

2.2.2 Octopus Perimetry

Octopus perimetry is one of the most widely used methods for detecting a visual field defect. It has the large white bowl with a radius of 30 cm and projects stimuli of different sizes and intensity (Bervers et al. 2019). This perimetry can not only perform standard static tests using 30-2, 24-2 and 10-2 patterns like in HFA, but it also provides two unique strategies: The G-

Program that tests the 30-degree field and is used for glaucoma assessment as well as the M-Program for analysing the macula area (in central 10 degrees).

A sensitivity Cluster Analysis is used in detection of glaucomatous visual field defects. It groups visual field defects according to the nerve fibre bundles. The cluster MD (mean defect) highlights the key pathological areas (Figure 6a). Moreover, the glaucomatous progression can be reflected by displaying the change of visual sensitivity (in dB/year) for each visual cluster: deterioration, improvement of sensitivity and fluctuation at both at 1% and 5% significance levels (Figure 6b).

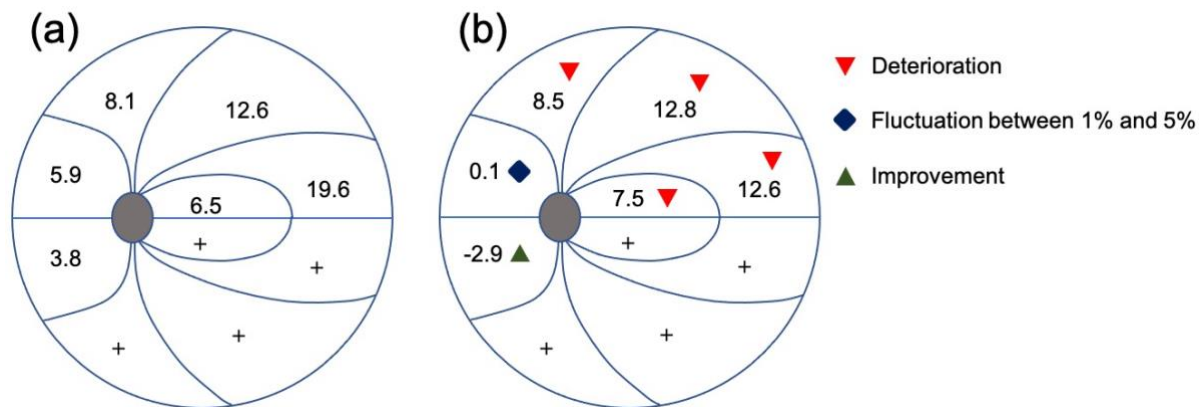


Figure 6. Cluster analysis of Octopus perimetry. a. Visual field defects are grouped according to the nerve fibre bundles. Numbers represent the cluster MD (mean defect). b. Cluster Trend shows the glaucomatous damage in every cluster. Deterioration was highlighted by red downward-pointing arrows. Green upward-pointing arrows represent improvement and blue diamonds show fluctuation at both at 1% and 5% significance levels.

Rowe et al recruited 126 patients of advanced glaucoma and performed VF test by Octopus 900. They found it was able to effectively detect the peripheral visual field loss. This is useful in clinical decision-making and disease monitoring in advanced-stage glaucoma (Rowe et al. 2021). Furthermore, Roberti et al improved Octopus perimetry, so that it could accurately detect a central visual field defect in an early glaucomatous eye (Roberti et al. 2017). In

summary, Octopus perimetry is capable of supporting routine glaucoma visual field testing and combine the central and peripheral visual field information to make the results more reliable.

2.2.3 Head-mounted automated perimeter ‘imo’

‘imo’ is a novel portable head-mounted perimeter. It consists of a head-mounted perimeter unit, a separate response button and a tablet which is controlled by the operator (Figure 7a). The perimeter unit is connected to the tablet via Wi-Fi and the response button is connected by Bluetooth (Figure 7a). Due to this wireless connection, the device is highly portable, and patients can be tested in any position they prefer. There are two separate optical systems (Figure 8b), one assigned to each eye. The device can measure the VF within 35° of the foveae(Matsumoto et al. 2016).

‘Imo’ uses an algorithm called Ambient Interactive ZEST (AIZE) which significantly reduces test duration(Kimura et al. 2019). HFA 30-2, 24-2 and 10-2 test patterns are compatible with ‘imo’, and it has its own unique test pattern “24 plus”. There are 78 test points in the 24 plus (1-2) test pattern which include 54 test points similar to the HFA 24-2 pattern (Figure 7c) plus an extra 24 test points in the central 10° VF (Figure 7d). Therefore, it provides more information about the central visual field loss compared to 24-2 pattern. 24 plus (1) test pattern emphasises the area corresponding to the retinal nerve fibre layer and includes 36 test points (Figure 8e)

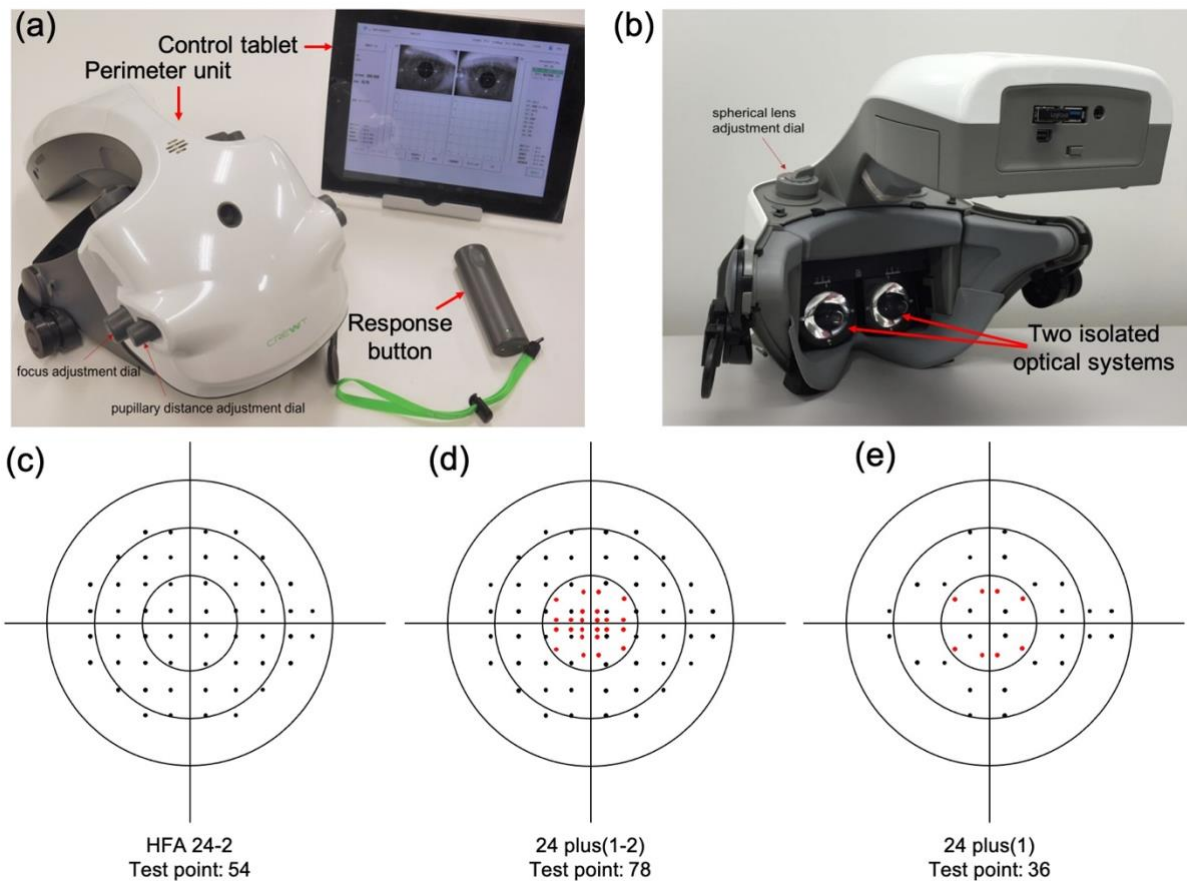


Figure 7. The images of ‘imo’ and the it’s test patterns. a. ‘imo’ consists of a main perimeter unit, a user control tablet, and a patient response button. Adapted with permission from Matsumoto et al. Copyright © 2016 Matsumoto et al. b. There are 2 totally isolated optical systems for the right and left eyes. Adapted with permission from Matsumoto et al. Copyright © 2016 Matsumoto et al. c. Test pattern of HFA 24-2, d. ‘imo’ 24 plus (1-2) and e. ‘imo’ 24 plus (1). HFA 24-2 test pattern has 54 test points. ‘imo’ 24 plus (1-2) adds 24 points within the central 10 degrees and has 78 test points. ‘imo’ 24plus (1) has 36 points.

‘imo’ can perform a monocular test that examines left and right eye separately because there are two separate testing systems (Figure 8a). The binocular random single-eye test mode is a novel approach. The stimulus randomly displays to either eye (Figure 8b), and both eyes can be generated from a single test. In addition, it can also perform a simultaneous binocular eye test. In this mode, a test target is shown in both eyes at a similar location, size and intensity

(Figure 8c)(Kumagai et al. 2020). ‘imo’ can track the pupil during the test and can correct for pupil deviation of ± 5 degrees. A study showed that this pupil tracking system can significantly stabilise the fixation compared to HFA(Goukon et al. 2019).

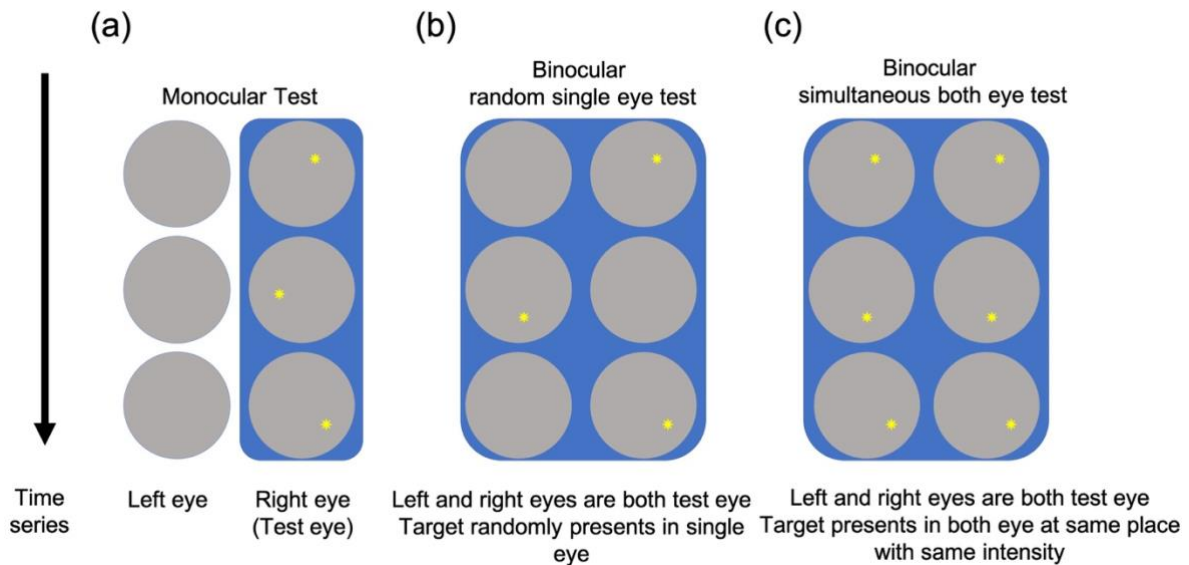


Figure 8. Test modes of imo. a. Monocular test examines left and right eyes separately without occlusion. b. Binocular random single-eye test: the test stimulus randomly presents to either eye, it examines both visual fields in both eyes simultaneously during a single examination c. In a binocular simultaneous test, the target presents simultaneously in both eyes at similar location, size, and intensity.

Since the development of imo, several studies have been done to evaluate its performance. Kimura et al compared both Global Indices and Reliability Indices obtained from HFA and imo. They found there was no significant difference between the MD obtained by HFA and imo. The average examination time was significantly shorter by 30.8% for imo ($10:54 \pm 2:19$ minutes) versus HFA ($15:23 \pm 2:07$ minutes) ($P < 0.01$) (Kimura et al. 2019). This suggests that reliable IOP measurements can be obtained faster with imo rather than HFA. Additionally, they also compared the data obtained when imo was head-mounted or fixed in a standing position and demonstrated that IOP measurements with imo are not significantly affected by

the position of the device(Kimura et al. 2019). ‘imo’ is a reliable device that can be used in every setting and provides an ideal approach for those unable to sit in the HFA. Further studies should be done to better determine the clinical potential of it.

Table 2. Summary of current device for visual field test.

Device	References	Performance parameter	Advantages of VF test	Limitations of VF test
HFA	(Wang and Henson 2013)	Sensitivity: 97.4% Selectivity: 58.6%	VF test is the routine test that directly reflect the function change. Devices like “imo” allow test being performed in any posture which make it suitable for certain patients.	HFA and Octopus are non-portable devices
Octopus	(Rowe and Rowlands 2014)	Sensitivity: 96% Selectivity: 55%		VF test is a subjective test, difficult to perform HFA in certain groups of patients such as children or the elderly.
imo	Kimura et al., 2019;	R ² of MD and VFI>0.81 for HFA vs imo		Learning effect that patients become familiar with VF test and increase false positive. Visual field defects are only noticed at advanced glaucoma

R²: Correlation coefficients

2.3 Optical coherence tomography

Visual function test such as visual field sensitivity test plays crucial roles in assessing the disease activity in glaucoma patients. However, some patients experience structural changes without any abnormalities in the VF(Tatham and Medeiros 2017). Therefore, it is value able to detect the of structural changes to assess the severity of glaucoma and determining the efficacy of treatment. The principle of OCT is somewhat like the ultrasound B that replaces sound with light. When a beam of light from the OCT is directed onto the retina, the retinal layers reflect and scatter the light. The structure is analysed by measuring the “echo” time delay, which is detected by correlation or interferometry techniques and intensity of backscattered light waves(Fujimoto et al. 2000). Several parameters can be obtained from the OCT include RNFL, ONH and macula parameters, which is known to be useful and effective measures of disease activity in glaucoma(Dong et al. 2016). All these parameters have their unique characteristics and are complementary to each other.

2.3.1 Retinal nerve fibre layer thickness

RNFL thinning caused by RGCs loss is one of the major hallmarks of glaucoma(Lee et al. 2016b). Wu et al indicated the RNFL thickness had great diagnostic capability for detecting glaucoma (Wu et al. 2012). Moreover, A study has shown that the change in RNFL thickness can be detected by OCT before the appearance of visual functional defects. Kuang et al included 75 eyes from 75 people with suspected glaucoma. Around 35% of eyes were found that had an abnormal average RNFL thickness 4 years prior to visual field loss. In 19% of the cohort, abnormalities in RNFL thickness preceded the VF loss by as much as 8 years(Kuang et al. 2015). Therefore, RNFL thickness has been shown to discriminate normal and glaucomatous eyes at early stages of the disease(Mwanza and Budenz 2016). The scanning area can be divided into “temporal-superior-nasal-inferior” areas(Figure 9)(Vazquez et al. 2021). A study indicated that the RNFL thickness of the inferior quadrant, clock-hour 7 segment as well as the total average thickness of the RNFL have greater diagnostic ability in detecting glaucomatous damage(Mwanza et al. 2011). Moreover, due to the high reproducibility, OCT RNFL progression analysis has a unique advantage in assessing glaucoma progression(Leung 2014).

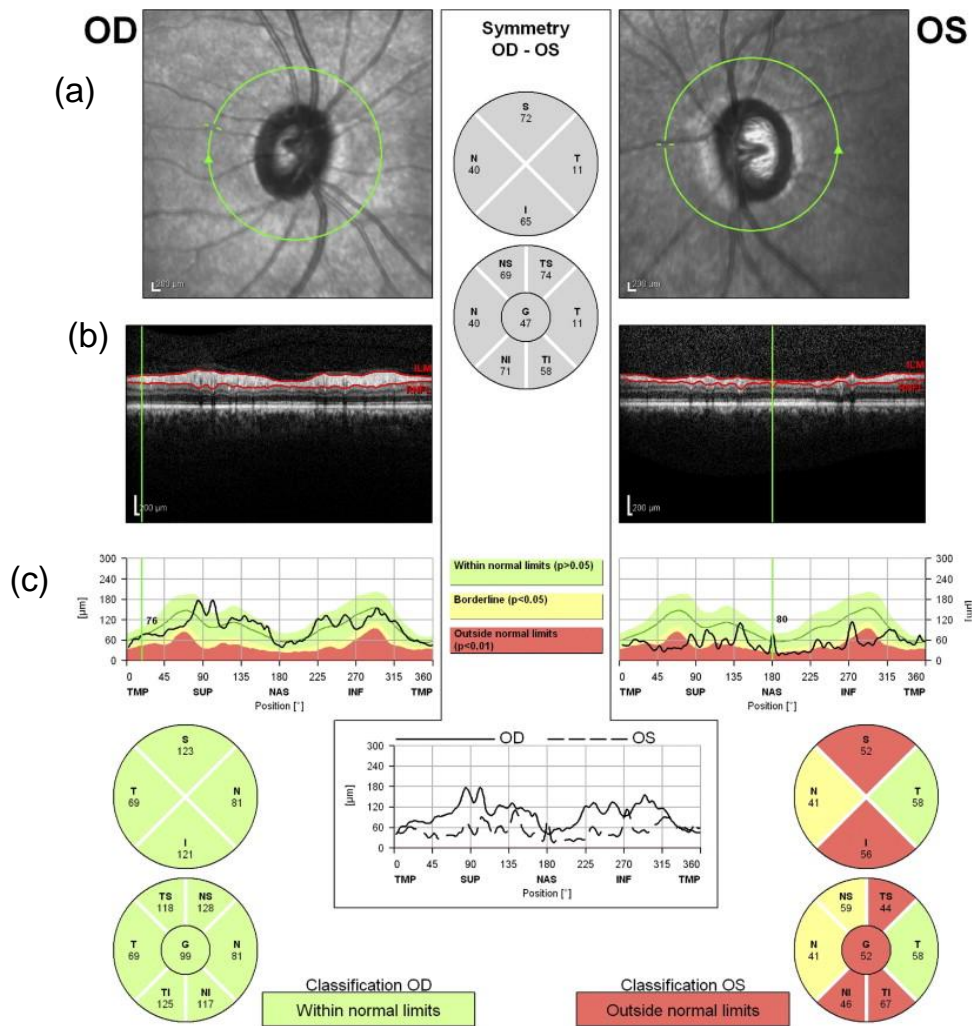


Figure 9. Report of the RNFL parameters. a. The scanning area of right and left eyes. (OD represent right eye and OS represent the left eye) And the area can be divided into “temporal-superior-nasal-inferior” pattern. b. The real image of retina. c. The analysis part of the report. In this example, the structure of right eye of the patient was normal. However, the RNFL thinning was recorded in superior and inferior quadrants. Adapted with permission from Wu et al. 2012 Copyright © 2012 Elsevier Inc.

2.3.2 Optic nerve head parameters

The optic nerve head, also known as the “optic disc” is the place where ganglion cell axons leave the eye. OCT produces detailed pictures of the ONH and can reflect the differences in the underlying structure. It provides information about the neuro-retinal rim (NRR) which represents the distance between the margin of the optic cup and head. Studies have shown that

the NRR measurement is a useful parameter to assess the severity of glaucoma and is very reproducible. Pilat et al indicated that the NRR area had great diagnostic abilities with PPV and NPV 82.8% and 83.3% , respectively(Pilat et al. 2019).

Bruch’s membrane opening (BMO) is a widely used parameter to estimate the structure of the ONH(Takada et al. 2016). The termination of the Bruch’s membrane at ONH forms an opening where retinal ganglion cells leave and form the outer border of optic nerve(Chauhan and Burgoyne 2013). This opening is called a “Bruch’s membrane opening”. Bruch's membrane opening–minimum rim width (BMO-MRW) is the minimal distance between the BMO and the internal limiting membrane (Miri et al. 2017) (Figure 10). It is valuable in estimating the glaucomatous damage of the ONH(Araie et al. 2017). It has already been proved that BMO-MRW has diagnostic power to reflect glaucomatous damages(Leaney et al. 2020) (Enders et al. 2018). Moreover, Enders et al found that the BMO-MRW was significantly reduced in patients with more severe visual loss(Enders et al. 2018). The horizontal rim width represents the distance between the BMO and ILM (Figure 11) and has the potential to help assess changes in the ONH structure(Muth and Hirneiss 2015). However, age is a factor that can affect the BMO-MRW as demonstrated by a study in Japan which found that BMO-MRW declined with age(Araie et al. 2017). Considering this, correlation of BMO-MRW and other BMO-based parameters should be adjusted to accommodate these factors.

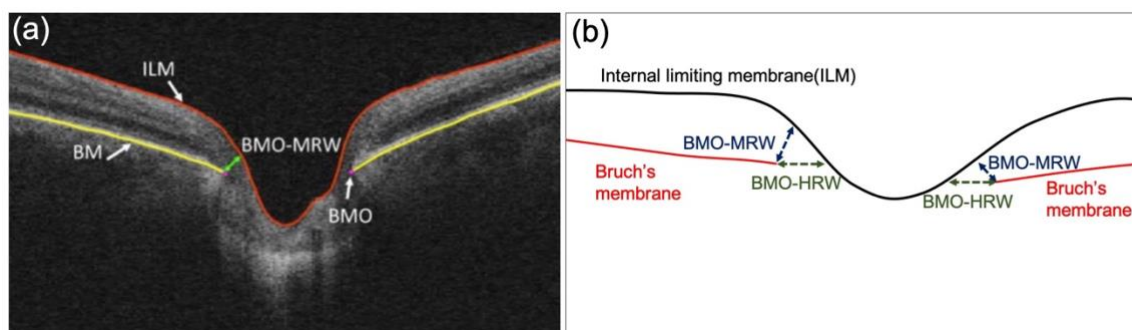


Figure 10. Diagram of BMO-based parameters. a. An OCT image showing the ILM and BMO. Adapted with permission from Miri et al. Copyright © 2017 Elsevier B.V.134 b. Schematic

illustration of BMO-based parameter: BMO-MRW which represents the minimal horizontal distance between the BMO and the ILM.

Macula parameters

The macular region accounts for less than 2% of the retina but contains over 50% of all RGCs making it susceptible to glaucomatous structural deficits(Hood et al. 2013). Development of the SD-OCT segmentation algorithms allows detection of individual layers within the macula(Bussel et al. 2014). The three innermost layers form the ganglion cell complex (GCC) which include the retinal nerve fibre layer (RNFL), the ganglion cell layer (GCL) and the inner plexiform layer (IPL) (Verticchio Vercellin et al. 2018). GCC-based parameters have already been proved to be reliable markers of structural change with high PPV of 98.9%(Garas et al. 2011). Moreover, the GCC thinning rate was also shown to correlate with the rate of visual function deterioration in glaucoma patients(Kuryshcheva and Lepeshkina 2021), which indicated GCC thinning could predict the functional loss.

It is known that a normal eye has inter-ocular and inter-hemispheric symmetrical properties i.e., the structure and function of each eye or hemisphere are similar. This symmetry could be affected in glaucoma, resulting in persistent asymmetry between glaucomatous eyes(Lee et al. 2016a). Based on this idea, a posterior pole asymmetry analysis (PPAA) was developed. The report of a PPAA test presents the central 24 degrees area divided into 64 (8×8 array) sectors centred on the fovea with the thickness of each area displayed (Figure 11a). The asymmetry map represents the difference in thickness between the corresponding cells in the left and right eyes (Figure 11b) as well as superior and inferior hemispheres (Figure 11c&d). The grey scales of asymmetry represent the difference between corresponding cells. The darker the shade, the bigger the difference(Pekel et al. 2015). A population-based experimental study looked at 122 eyes in healthy and glaucoma subjects in different stages. The AUC of asymmetry indices for preperimetric, early and advanced glaucoma patients were 0.773–0.994, 0.861–0.998 and

0.819–0.996 respectively(Yamada et al. 2014a). The asymmetry index was effective in distinguishing between a normal eye and varying stages of glaucoma, in particular the index of the ganglion cell layer (with AUC 0.994–0.998)(Yamada et al. 2014a). Lee et al produced similar results, suggesting that the PPAA was able to serve as a potential tool to estimate disease activity(Lee et al. 2016a). Moreover, PPAA can accurately distinguish between normal people and PACG patients even without any specific symptoms such as vision loss or increased intraocular pressure (IOP), suggesting that PPAA could be an indicator of PACG (Zha et al. 2019).

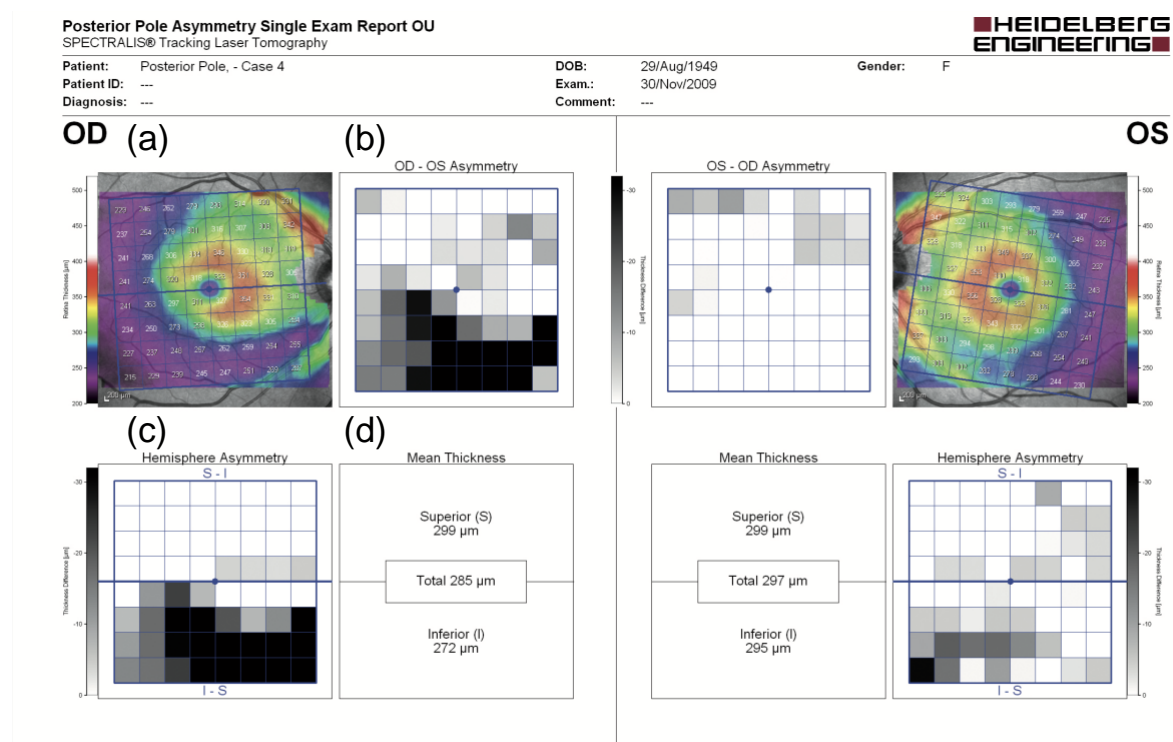


Figure 11. A posterior pole asymmetry examination report. a. The colourful 8x8 analysis grid graph displaying the central 24 degrees divided into 64 (8x8 array) sectors centred on the fovea. The number in each cell represents thickness. b. OD-OS and OS-OD asymmetry analysis report. The thickness of cells between eyes are compared. c. The hemisphere asymmetry analysis grey scale. d. Mean retinal thickness of superior and inferior hemisphere. Image courtesy of Heidelberg Engineering.

The OCT parameters are all able to estimate the structural damage and monitor disease progression with good accuracy and reproducibility (Table 3). Due to advancements in the imaging technology and improved algorithms, the OCT graphs have become more accurate and with better resolution. Further developments in the analysis of these parameters could enrich our understanding of glaucoma. OCT is an indispensable tool to estimate disease progression and monitoring in glaucoma.

Table 3. Summary of OCT parameters

Parameter	Reference	AUC	PPV and NPV %	Sensitivity & specificity %	Advantages of OCT test	Limitations of OCT test
RNFL thickness	Wu et al. 2012	0.952	PPV: 89.1 NPV: 86.8	Sensitivity: 80.3 Specificity: 92.9	OCT test is an objective test and quantify the structure change. Development of algorithms improve the accuracy and resolution.	The co-operation and responses of patients are required. Requirement for well-trained operators.
NRR area	Pilat et al. 2019	-	PPV: 82.8 NPV: 83.3	Sensitivity: 88.9 Specificity: 75.0		
BMO-MRW	Leaney et al. 2020	0.95	PPV: 86.0 NPV: 94.0	Sensitivity: 89.0 Specificity: 93.0		
GCC	Garas et al. 2011	-	PPV: 98.9 NPV: 47.6	Sensitivity: 48.2 Specificity: 98.9		
PPAA	Yamada et al. 2014a	0.994-0.998	-	-		

3. Advanced Technologies for Glaucoma Measurement

The clinical tests discussed so far have been used in clinical practice for decades. However, studies continue to investigate other possible measures of disease activity, with several recent developments (Normando et al. 2020; Shpak et al. 2018). There has been an enormous advancement in tear fluid investigation. Paper-based microfluidic devices and contact lenses provide excellent platforms to rapidly detect and analyse the tear fluid components (Yetisen et al. 2017). Another development is DARC which is a novel technique that directly reflect the survival of retinal ganglion cells by using fluorescent dye allowing dead cells to be quantified (Normando et al. 2020). AI provides a platform to analyse a huge amount of data and to improve the accuracy. In this section, we will discuss several technologies that have potential in the detection and monitoring of glaucoma.

3.1 Tear fluid analysis and molecular biomarkers of glaucoma

Tears are a complex mixture composed of electrolytes, water, proteins, mucin, and lipid (Moshirfar et al. 2014). Recent proteomic studies have shown that there are approximately 1500 types of proteins in tears(Hagan et al. 2016). As the “proximal fluid” consists of tear film which covers the eye surface, tears may directly reflect ocular disorders(Hagan et al. 2016). Several studies have indicated that changes in certain components are related to glaucoma(Ghaffariyeh et al. 2009; Sahay et al. 2017; Shpak et al. 2018). These molecules can be considered to be biomarkers.

Aiming to improve the early assessment of disease activity, biomarkers are currently a hot topic in research(McNally and O'Brien 2014). Biomarkers are able to predict the severity and course of the disease at early stage(Bhattacharya et al. 2013). Although not all pathogenic mechanisms of glaucoma are well understood, certain factors involved in the disease process have been identified. These include neurodegeneration, immune reaction, ischemia, and oxidative stress(Beykin and Goldberg 2019). The concentrations of molecules related to these processes are different in glaucoma patients when compared to healthy individuals. Therefore, these molecules may serve as potential biomarkers of glaucoma. There are several sources of biomarkers, including tears, aqueous humour and blood(Dammeier et al. 2018; Oddone et al. 2017; Pan et al. 2020). However, obtaining a sample of aqueous humour or blood, is an invasive and complex procedure limiting their use. Considering this, tears have the potential to be an ideal resource for biomarker analysis due to the ease with which they can be collected.

3.1.1 Molecular biomarkers

BDNF is a type of regulatory protein in the central nervous system and helps to promote proliferation, differentiation, survival and functioning of neurons(Shpak et al. 2018). BDNF is produced in the superior colliculus and transported to retinal ganglion cells via a retrograde axonal transportation system (Ghaffariyeh et al. 2009). Damage to the optic nerve axons blocks

the retrograde axonal transportation system(Mysona et al. 2017). Therefore, tear levels of BDNF may be very useful in assessing disease activity in glaucoma.

Ghaffariyeh et al was first to measure and compare the BDNF concentration in tears of healthy and normal tension glaucoma (NTG) eyes(Ghaffariyeh et al. 2009). They found mean concentration of BDNF in normal people was 77.09 ± 4.84 ng/ mL, compared to 24.33 ± 1.48 ng/mL in NTG patients (Ghaffariyeh et al. 2009). Findings demonstrated that the BDNF concentration was significantly lower in patients with normal tension glaucoma with $P < 0.05$. Shpak et al focused on patients with POAG (Shpak et al. 2018). They found that the concentration of BDNF in tears of POAG patients was 78.0 ± 25.1 pg/mL, compared to 116.2 ± 43.1 pg/mL in the control group with $P < 0.001$. The trend of decreased BDNF in glaucomatous eyes was similar to the previous study. In addition, they were able to detect varying levels of tear BDNF in eyes at different stages of POAG. The results showed a pronounced decline in BDNF in the early stage of POAG with a relative increase in BDNF levels in following stages. The concentration in blood serum and aqueous humour showed the same trend(Shpak et al. 2018).

Matrix metalloproteinases (MMPs) are a group of protein play important roles in remodelling the extra cellular matrix in the trabecular meshwork. Interestingly, MMPs are also involved in the death of RGCs and changes in MMPs levels are seen in glaucoma(Singh et al. 2015). Several studies demonstrated the link between MMPs and glaucoma. Sahay et al tested the difference in expression of MMP 2 and 9 in tears from 113 patients with different subtypes of glaucoma and compared them with normal people(Sahay et al. 2017). Results indicated that both activity and expression levels of MMP 9 were significantly increased in primary glaucoma, especially in the early stage ($P < 0.001$)(Sahay et al. 2017). Another study found the overexpression of MMP 9 was also observed in POAG patients(Kim et al. 2021).

The role of immune system in glaucoma pathologies has attracted increasing attention (Rieck 2013; Tezel and Wax 2004). Immune response and inflammation induced by glial cells such as astrocytes, Muller cells and microglia is also related to glaucomatous damage (Chen et al. 2018) (Adornetto et al. 2019). Therefore, factors related to these inflammatory responses may serve as biomarkers of glaucoma. Chua et al indicated that the levels of interleukin (IL)-9, IL-10, IL-12, interferon (IFN)- α , IFN- γ , and monokines induced by interferon-gamma were significantly raised in glaucomatous eyes (Chua et al. 2012) Moreover, proteomics identified some factors involved in inflammation and immune response including beta-2-microglobulin, heat shock protein beta-1, Ig alpha-1 chain C region, Ig alpha-2 chain C region, immunoglobulin J chain, Ig kappa chain C region, Lactotransferri, lysozyme C, polymeric immunoglobulin receptor, serotransferrin and serum albumin. All of them are overexpressed in tears from patients with POAG (Pieragostino et al. 2013).

Mucins are types of glycoproteins that form a major part of tear fluid. MUC5AC is a main component of the tear film. A study demonstrated that MUC5AC concentration was significantly downregulated in glaucoma patients compared with healthy people, with the mean concentration of 16.95 ± 12.86 ng/ml and 32.39 ± 18.44 ng/ml respectively ($p < 0.05$) (Liu et al. 2010). Furthermore, Roedl et al. investigated the role of Homocysteine (Hcy), which is an amino acid involved in pathological changes in glaucoma. They reported that the Hcy level in tears from glaucomatous eyes was 205 ± 84 nmol/L, compared with 130 ± 53 nmol/l in the control group which indicated that the Hcy expression was higher in POAG patients (Roedl et al. 2008).

Notably, research into molecular biomarkers has undergone a revolutionary change in recent years. There is rising interest in non-invasive methods of detecting biomarkers in patients, with tear fluid analysis becoming an attractive option for measuring disease activity. Technological advances have facilitated the analysis of tear composition. Some of the components may serve

as biomarkers of glaucoma, however, it is necessary to characterise the normal concentration range of molecules in healthy people. All things considered; further studies should be done to identify a molecular biomarker which can be used clinically.

3.1.2 Tear fluid analysis platforms

Tear fluid analysis tests have been present for a long time. The first ones were developed over a hundred years ago, such as Schirmer's test for tear volume measurement(Saleh et al. 2006). Phenol red thread test was also introduced at that time and was used to detect the tear volume based on the pH value(Tomlinson et al. 2001). More recently, new devices have been developed that can rapidly detect and analyse the tear fluid components.

Lateral flow assay (LFA) is one of the broadly used devices in rapid diagnostics (Yetisen et al. 2013). LFA strips are made of several parts including a sample pad, conjugate pad, reaction membrane and absorbance pad(Koczula and Gallotta 2016). The liquid sample is introduced onto the sample pad and migrates to the conjugate pad (Figure 12a). The conjugate pad is impregnated with labelled antibodies which can interact with analytes in the sample. The labelled analytes then migrate to the reaction membrane where antibodies for the desired analyte are fixed at a certain area (test line), if the sample contains the desired analyte they are captured at this area and form a visible line indicating a positive test (Figure 12b)(Koczula and Gallotta 2016; Miocevic et al. 2017; Yetisen et al. 2013). InflammDry (Figure 12c&d) is a LFA device that is able to measure MMP-9 level in the tear fluid with great sensitivity (85%)(Bang et al. 2020; Sambursky et al. 2013). Several studies demonstrated InflammDry was able to provide reliable results reflective of patients' symptoms(Messmer et al. 2016; Sambursky et al. 2014). Notably, this study also indicated that untrained operators were capable of performing the InflammDry test successfully. One of the major advantages of tear fluid analysis is the health economics. Due to its low cost (for example only \$16 per InflammDry test), short response time, clear visual results, long shelf life and the fact that refrigeration is

not required for storage, LFA has a great potential to be a novel point-of-care diagnostic tool. However, most LFA devices only provide qualitative or semi-quantitative results. Specialized reading devices are strongly required to quantify certain analytes, but the cost and response time will also increase. On the other hand, it is a big challenge to preparing the sample for LFA test.

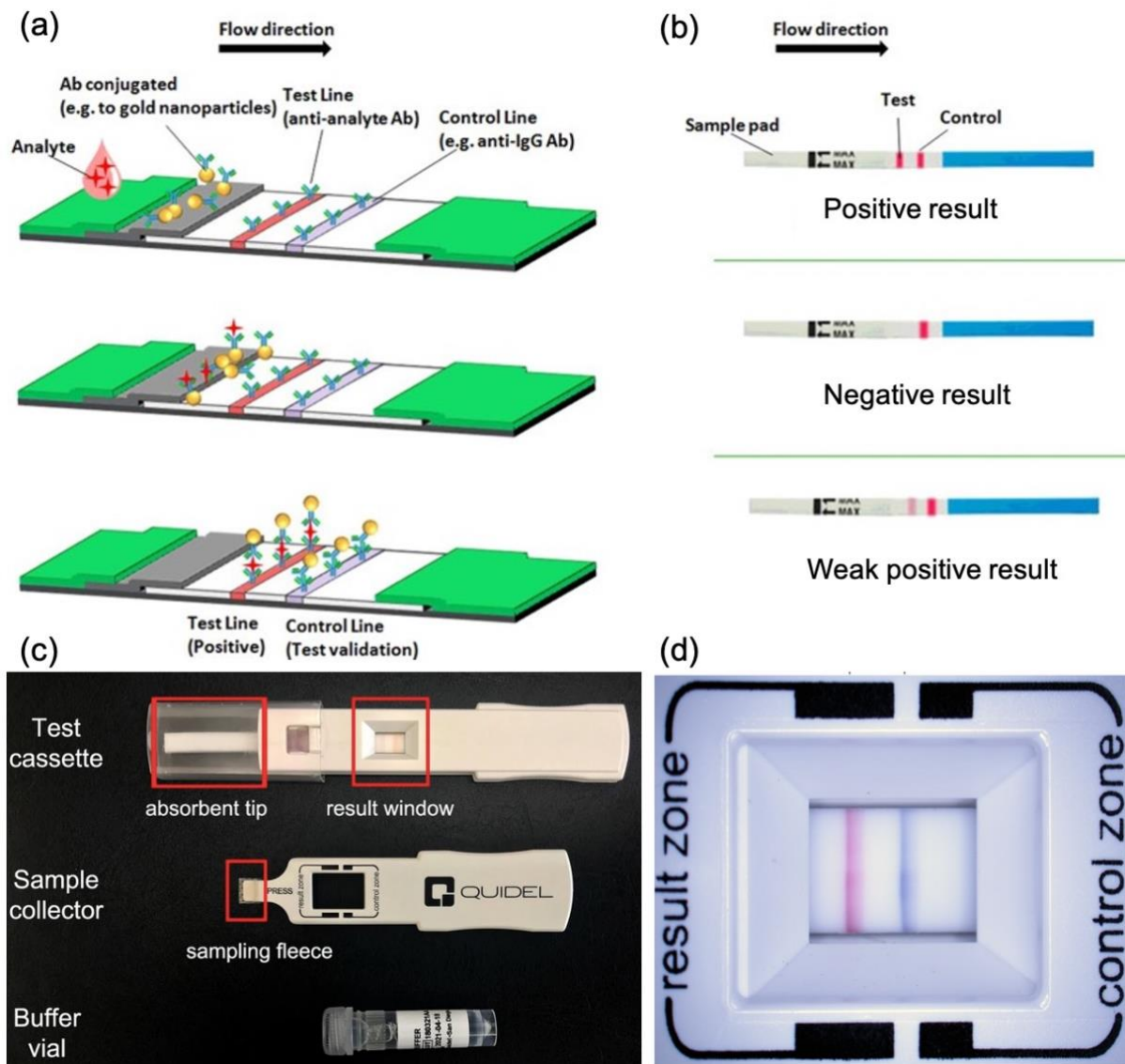


Figure 12. Lateral flow assay. a. Schematic illustration of a typical ILFA strip. Labelled antibody is packed in the conjugate pad. The liquid sample containing certain analytes is introduced at the sample pad and subsequently released onto the conjugate pad. Then, the labelled analytes move to the reaction membrane, where the bound target analyte is captured

at the test line. Adapted with permission from Koczula and Gallotta. Copyright © 2016 Katarzyna M. Koczula et al. b. A commonly used LFA strip and possible results of test. Adapted with permission from Koczula and Gallotta. Copyright © 2016 Katarzyna M. Koczula et al. c. InflammDry LFA test kit. The kit contains a test cassette, sample collector and a vial of buffer. Adapted with permission from Bang et al. Copyright © 2020 Seung Pil Bang et al. d. The result zone of InflammDry. A red test line represents the concentration of MMP-9 is higher than 40 ng/mL. And A blue control line indicates that the test is valid. Adapted with permission from Bang et al. Copyright © 2020 Seung Pil Bang et al

Numerous studies have focused on improving paper-based analytical devices μ PAD (Sonobe et al. 2019; Yamada et al. 2014b). μ PAD contains a hydrophilic paper platform, and hydrophobic barriers which allows the liquid sample can then easily flow through the μ PAD (Lam et al. 2017). Due to low-costs as well as simple, safe and requiring a small sample volume, μ PAD could be successfully used in several areas(Yamada et al. 2014b). Yamada et al used μ PAD (Figure 13a) to quantify the concentration of lactoferrin in tears. Inkjet printing technology was used to form the hydrophilic channel. Terbium (Tb^{3+}), which binds lactoferrin, was deposited onto the paper to generate detectable fluorescent emission, reflecting the concentration of lactoferrin(Yamada et al. 2014b). Moreover, the production cost of each μ PAD was only \$0.013(Yamada et al. 2014b). Yetisen et al introduced a paper-based microfluidic device (Figure 13b) for quantitative analysis of electrolytes (Na^+ , K^+ , Ca^{2+} ions) in tears(Yetisen et al. 2017). The device provided the diagnostic results within only 3 minutes. Moreover, smart phones camera could be used to capture the image of colour change of test strips. ImageJ was then used to quantify the coloristic change(Yetisen et al. 2017). The μ PAD can provide objective evidence of underlying ocular diseases. However, analytic devices are required to improve its accuracy and sensitivity.

Contact lenses are a commonly used optical device (Moreddu et al. 2019). Recently, they have showed a potential as a platform for tear analysis due to its relatively non-invasive properties and its ability to provide real-time monitoring of tears (Park et al. 2018a). Yetisen et al introduced a contact lens device capable of detecting electrolytes in tears (Yetisen et al. 2020). Moreover, Moreddu et al integrated biosensors within the contact lenses (Figure 13c). This allowed for the multiplexed detection of tear components, including: proteins, glucose, nitrites, and the pH value (Figure 13d) of tear within 5 seconds (Moreddu et al. 2020). Contact lens devices is able to be valuable point-of-care fluid analysers capable of monitoring a range of ocular diseases including glaucoma. However, the possible adverse effects of wearing contact lenses, such as discomfort, microbial keratitis, and other corneal complications must be taken into consideration.

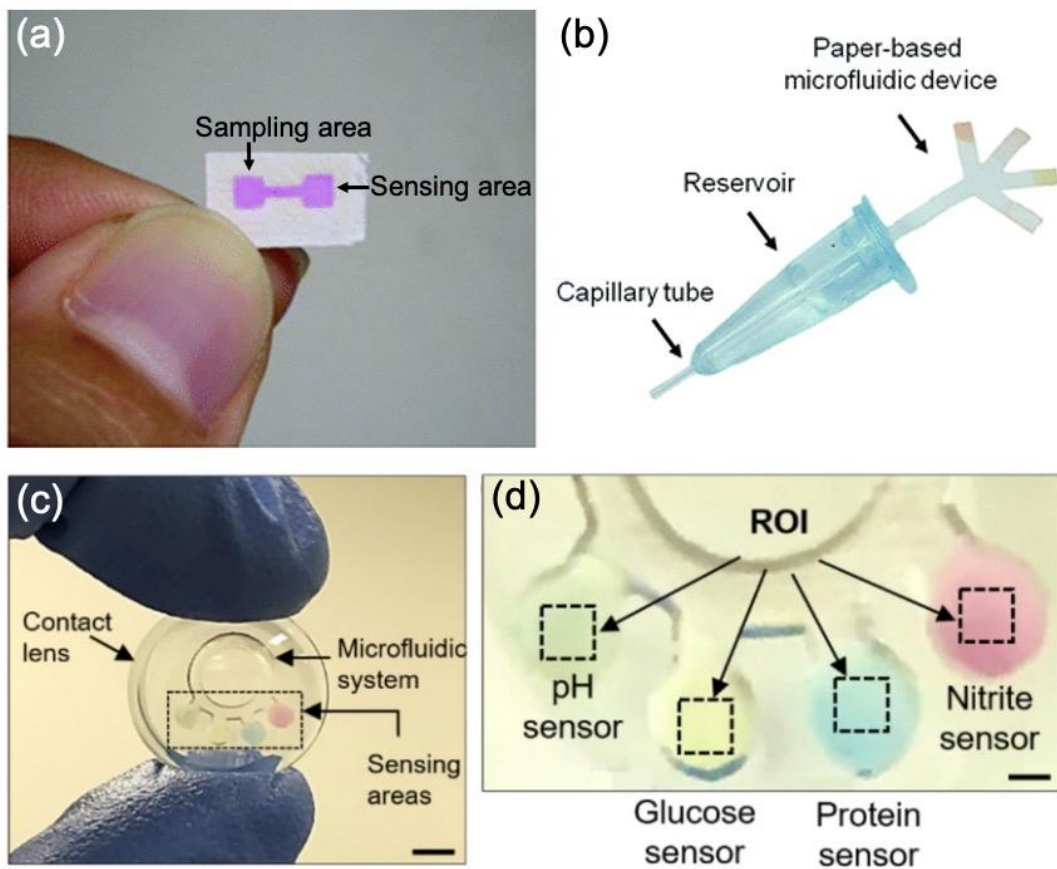


Figure 13. μPAD and contact lens device for tear analysis. a. A μPAD device patterned by inkjet printer. Two similar square areas were used for sample deposition (sampling area) and

sample reaction (sensing area). Adapted with permission from Yamada et al. Copyright © 2014 RSC publishing. b. A paper-based microfluidic device developed to analyse the electrolytes in tears. Tear fluid was collected by a capillary tube and temporarily stored in a reservoir. Adapted with permission from Yetisen et al. Copyright © 2014 RSC publishing. c. A contact lens with different sensors. Scale bar: 5.0 mm. Adapted with permission from Moreddu et al. Copyright © 2020 Elsevier B.V. d. Sensors were embedded in the contact lens. The pH value and concentration of glucose, protein and nitrate were indicated by colour. Scale bar: 1.0 mm. Adapted with permission from Moreddu et al. Copyright © 2020 Elsevier B.V.

Table 4. Summary of Tear fluid analysis platforms

Technique	Reference	Analytes	Sensitivity/LOD	Advantages	Limitation
InflammaDry (Lateral flow assay)	Bang et al. 2020; Sambursky et al. 2013	MMP-9	85%	Cheap: \$16 per test Fast: 10mins per test Easy-to-use clear visual results long shelf life	Need to prepare sample before test. Specialized reading devices are required to quantify analytes.
μPAD	Yamada et al. 2014b	Lactoferrin	LOD: 0.30 mg mL ⁻¹	Cheap: \$0.0131 per uPAD Fast: 15 mins per test Small sample volume	Specific reading devices are required to improve the accuracy and repeatability.
	Yetisen et al. 2017	Electrolyte	Na ⁺ sensor: 2.7 mmol L ⁻¹ K ⁺ sensor: 1.4 mmol L ⁻¹ Ca ²⁺ sensor: 0.02 mmol L ⁻¹	Fast: response in 3 secs Low-cost Multiple analytes get tests similarity Sensitive	
Contact lens	Yetisen et al. 2020	Electrolyte	Na ⁺ sensor: 6.7 mmol L ⁻¹ K ⁺ sensor: 0.8 mmol L ⁻¹ Ca ²⁺ sensor: 0.02–0.05 mmol L ⁻¹ Mg ²⁺ sensor: 0.10–0.44 mmol L ⁻¹	Fast: response in 5 mins Multiplexed detection of tear components Cost-effective Sensitive	May cause adverse effects such as discomfort, microbial keratitis, and other corneal complications.
	Moreddu et al. 2020	pH; glucose; protein; nitrite ions	pH sensor: 12.23 nm/pH unit Glucose sensor: 1.4 nm/mmol L ⁻¹ Protein sensor: 0.49 nm/g L ⁻¹ Nitrites sensor: 0.03 nm/μmol L ⁻¹	Fast: response in 15 secs Sensitive Suitable for point-of-care settings	

LOD: The limit of detection

3.2 Detection of Apoptosing Retinal Cells (DARC)

RGCs death and the optic nerve loss are the major characteristics of glaucoma. It is reported that approximately 20–40% of the RGCs have already been lost before the visual defect becomes apparent(Ahmad 2017). RGC death is caused by several pathological events including ischemia or axonal injury. RGCs can also undergo programmed cell death: apoptosis(Ahmad 2017). The RGCs subsequently shrink, membrane blebbing takes place, chromatin is condensed and pyknotic nuclei develop. Phosphatidylserine (PS) is believed to be one of the markers of apoptosis(Yap et al. 2020b). PS is usually located in the inner leaflet and asymmetrically distributed across the cell membrane. When the RGCs undergo apoptosis, more PS starts to appear on the outer leaflet (Figure 14)(Ahmad 2017; Yap et al. 2020b).

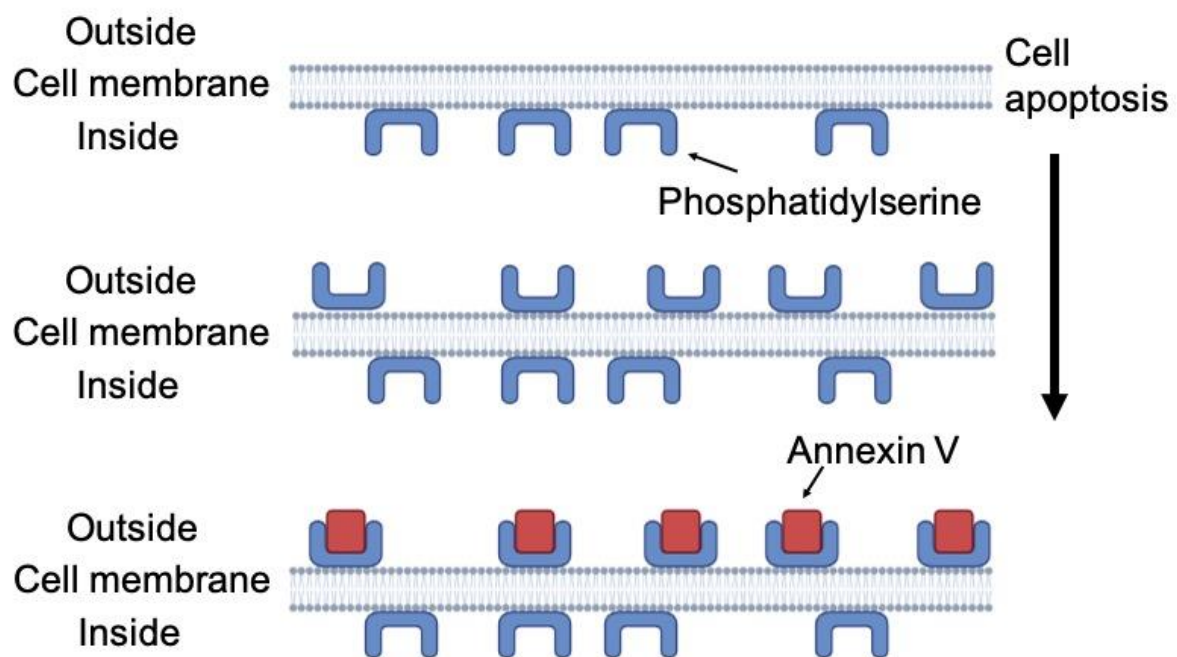


Figure 14. Diagram of phosphatidylserine location and annexin V binding. Phosphatidylserine (PS) is located in the inner leaflet of cell membrane. More PS appears on the outer leaflet when apoptosis start. Annexin A5 has a high affinity for PS.

DARC is a technique that allows the identification and visualisation of apoptosing RGCs by using fluorescently labelled annexin A5 (Yap et al. 2018b). Annexins use calcium (Ca^{2+}) to bind to phospholipids. Annexin A5 has a high affinity to PS. Therefore annexin A5 is regarded as an ideal indicator of an apoptosing cell (Normando et al. 2013). In DARC, the annexin A5 is conjugated with either a 488 nm (ANX488) or 776 nm (ANX776) fluorophore. In humans, the dye is administered intravenously. The annexin V-bound fluorophore is then excited by a laser and a photodetector system is used to detect the fluorescent light emission. A confocal scanning laser ophthalmoscope (cLSO) is required to analyse the retina (Bizrah et al. 2014; Yap et al. 2020b).

DARC has already been used in rat studies including an intravitreal staurosporine-induced model and some transgenic murine models. According to these studies, the RGC apoptosis was successfully visualised by DARC. Moreover, DARC was also used to analyse the pathogenesis of neurodegeneration. Interestingly, effects of novel agents such as memantine can be investigated by assessing RGC with this technology (Yap et al. 2018a). A human trial was also performed. It involved 8 patients with progressing glaucoma and 8 healthy people. Both groups received intravenous injections of fluorescent labelled annexin 5. The doses ranged from 0.1, 0.2, 0.4 to 0.5 mg. Results showed the DARC counts (the total number of unique ANX776-labelled spots) was significantly increased in glaucoma patients. Furthermore, ANX776 was proved to be safe and did not cause any serious adverse events (Cordeiro et al. 2017).

In summary, DARC provides a promising method to directly measure structural changes in RGCs and improve understanding of the cellular mechanisms involved in the development of RGC degeneration. Importantly, DARC significantly reduce the detection time of glaucoma because the Annexin V binding only takes a few minutes (Ahmad 2017). However, further human studies are required.

3.3 Artificial intelligence (AI) in glaucoma

AI is an artificial entity capable of performing certain human tasks such as decision making and recognition of the features of certain subjects(Zheng et al. 2019). AI has flourished in recent times. Previously, computers could only execute instructions by a series of if-then statements programmed by a human. Advances in AI has led to Machine Learning (ML), whereby a computer can learn patterns of data rather than being programmed. However, it was not until Deep Learning (DL) algorithms were developed in 2010 that AI became more widely used in medicine (Salazar et al. 2021). DL is a subfield of ML. The artificial neural networks (ANN) form the backbone of DL. The ANN imitates the biological information processing pattern of the human brain. ANN consists of input layers, output layers and one or more intervening layers. A simple mathematical operation is regarded as an “artificial neuron” and several “neurons” form different layers(Mayro et al. 2019; Wu and Feng 2017). The “deep” in DL actually refers to the depth of intervening layers which significantly improve the data analysis ability of DL(Salazar et al. 2021). Convolutional neural networks (CNN) are a type of DL construct particularly suited to recognising images(Salazar et al. 2021). The input or the image undergoes feature extraction and classification, this data is processed and the results are output (Figure 15). Features (such as special tissue or pathology) are extracted by several hidden layers following the input layer. The hidden layers work in hierarchy, so a hidden layer analyses the features extracted by the previous layer, with more layers allowing the extraction of more sophisticated features(Kaur and Khosla 2020).

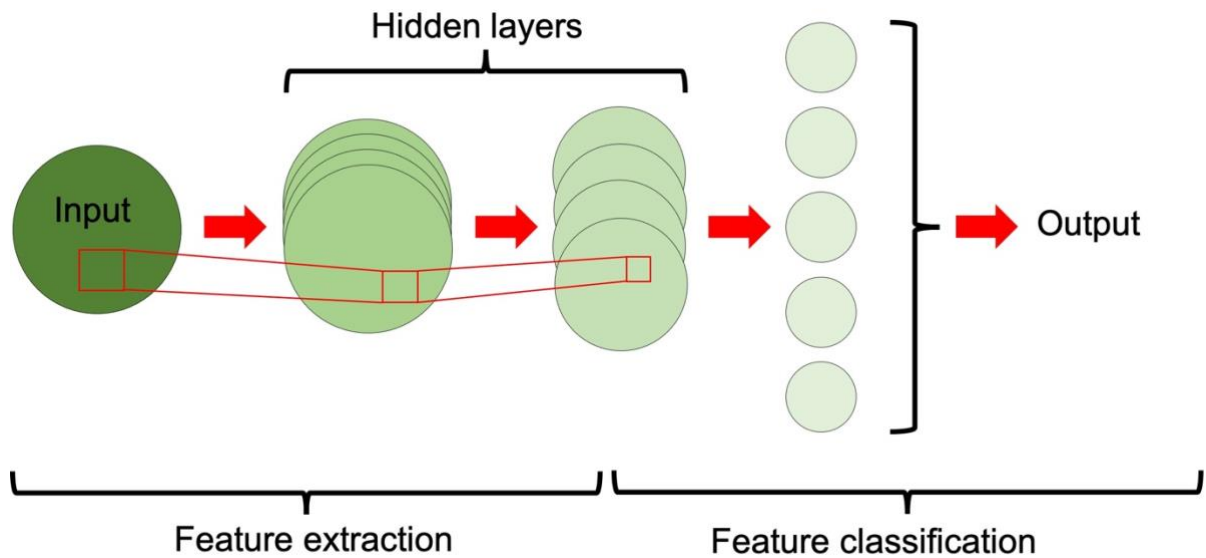


Figure 15. Diagram of Convolutional neural networks. In the convolutional neural network framework (CNN) portions of the image (red box) are reduced into mathematical representations and features are analysed in the hidden layers. Features are characterised by data and similar data is combined. Several repetitions in multiple layers produce the final output.

An important part of AI is data volume and due to the retinal imaging and functional data in ophthalmology comprising big datasets, there have been increasing interest in using AI for diagnostic and prediction in diseases such as glaucoma.

3.3.1 AI for glaucoma diagnosis

Measures of disease activity in glaucoma are based on assessing the structural and functional damage using techniques such as IOP, VF test, fundus images and OCT(Prabhakar et al. 2021). However, analysis of the results of these investigations poses a challenge and is dependent on the experience of doctors with differing opinions leading to disagreements in management(Wang et al. 2019). AI has been shown to have a significant potential in assisting complex data and image analysis which allow AI to differentiate glaucomatous functional and/or structural changes form normal eyes(Zheng et al. 2019).

VF testing is a routine test to measure the disease activity in glaucoma because it directly assesses visual function. The application of computer algorithm in automated visual field testing is a significant advancement(Mayro et al. 2019). Algorithms provide several reliability parameters, a numeric figure of visual sensitivity and global indices which improve the accuracy of VF test. Recently, AI has been shown to be capable of differentiating glaucomatous visual field from normal eyes(Zheng et al. 2019). Goldbaum et al firstly developed a two-layer artificial neural network for the analysis of the visual field damage in 1994 and the results were comparable with the diagnosis provided by 2 specialists (Goldbaum et al. 1994). In the subsequent studies, huge number of AI systems were developed. For instance, Kucur et al developed a CNN algorithm that differentiated glaucoma patients from normal people with great average precision of 0.874 ± 0.095 (Kucur et al. 2018). Li et al also introduced a DL algorithm that detected glaucomatous change with the accuracy of 0.876, and the accuracy was higher than other machine learning models(Li et al. 2018a).

Assessing structural change plays important roles in diagnosis of glaucoma. Fundus photographs is one of the simplest methods to assess structural change of optic disc and plays important roles in glaucoma screening(Benzebouchi et al. 2018; Mursch-Edlmayr et al. 2020). Combining AI with fundus photography has already been proved to be a powerful approach to measure the structural change. For instance, Raghavendra et al developed a eighteen-layer CNN system which was able to significantly detected the glaucomatous structural changes from fundus photography(Raghavendra et al. 2018). The system was trained in 1426 images and the accuracy reached to 98.13% with PPV (positive predictive value) of 98.79%(Raghavendra et al. 2018). Li et al enlarged their training set to 48000 fundus photographs which allowed their DL systems detect the optic neuropathy accurately (Li et al. 2018b; Liu et al. 2019).

OCT is regarded as the standard measures of assessing structural damage in glaucoma due to its accuracy and reproducibility. Many AI programs have been developed for the analysis of OCT images(García et al. 2020). One example is a DL algorithm developed to assess the RNFL thickness(Ran et al. 2019). The algorithm was able to analyse the OCT images and generated heatmaps which indicated the glaucomatous neuropathy area (Figure 16) (Ran et al. 2019). Li et al introduced a AI system which was able to adjust the influence of age, gender, and ocular biometric parameters and improve the accuracy of diagnosis based on RNFL thickness(Li et al. 2021). García et al introduced a deep learning system which could highlight the glaucomatous structural change in the circumpapillary OCT images(García et al. 2020). Devalla et al developed a DL algorithm analysed ONH from OCT images which has been proven to perform well in differentiating glaucoma from normal individuals, with high sensitivity, specificity and accuracy(Devalla et al. 2018). Another study focused on BMO-MRW. Thompson et al. developed a deep learning algorithm to quantify the glaucomatous damage of optic nerve via BMO-MRW(Thompson et al. 2019). It showed a high accuracy (0.945 AUC) in detecting and glaucoma(Thompson et al. 2019). Moreover, there are also several programs which have been developed to measure the disease activity in glaucoma using a macular vessel density, optic disc, and cup parameters(Miri et al. 2015; Park et al. 2018b).

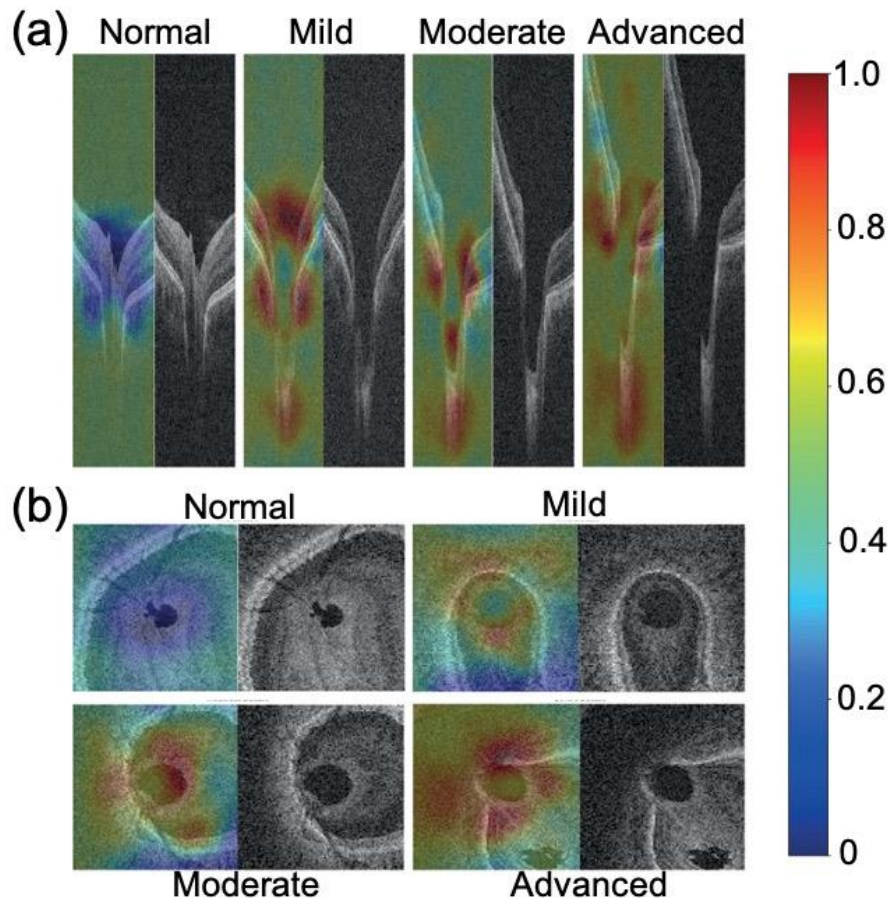


Figure 16. Examples of OCT images and corresponding heatmaps of normal, mild glaucoma, moderate glaucoma and advanced glaucoma. a. The cross-sectional OCT images and heatmaps. b. The en face OCT images and heatmaps. The value of 1 (red) indicate the greatest diagnosis ability to discriminate glaucomatous damage, whereas the 0 (blue) represent the greatest diagnosis ability to discriminate normal tissue. Adapted with permission from Ran et al. Copyright © 2019 Ran et al. Published by Elsevier Ltd.

To improve the discriminatory power of AI, some research groups tried to combination functional and structural damage. One study trained the ANN on the optic nerve head (ONH) parameters and VF indices. They found that the accuracy of the ANN was higher when trained with both parameters (88%) than trained with only one parameter (80% for the ONH parameter and 84% for VF indices)(Devala et al. 2020). Kim et al built several AI modals which were able to combine the data of RNFL thickness and visual field(Kim et al. 2017b). Even though it

is challenging to train AI on both functional and structural parameters, such AI models show impressive performance for glaucoma detection. Apart from functional and structural damage in glaucomatous eyes, researchers also focused on combination of genetic data to develop a new approach for glaucoma assessment(Devalla et al. 2020).

3.3.2 AI for prediction in glaucoma progression

Prediction the progression plays important roles in management of glaucoma. To predict the progression, patients could receive several tests over lots of visits, and managing these data is time consuming and requires the expertise of clinicians(Devalla et al. 2020). Several studies have evaluated the accuracy of AI in the forecasting of glaucomatous disease. For instance, Wen et al indicated the deep learning network could forecast the visual field loss(Figure 17)(Wen et al. 2018). They developed, trained and tested the DL network with the results of 24–2 Humphrey Visual Field test from 1998 to 2018 from a university database. The model successfully forecasted visual field of glaucoma patients up to 5.5 years. The average difference between predicted and actual loss was only 0.41 dB and the correlation of mean deviation (MD) was 0.92(Wen et al. 2018). Similarity, Yousefi et al indicated that machine learning was capable of detecting glaucoma progression early even for slowly progressing eyes(Yousefi et al. 2018).

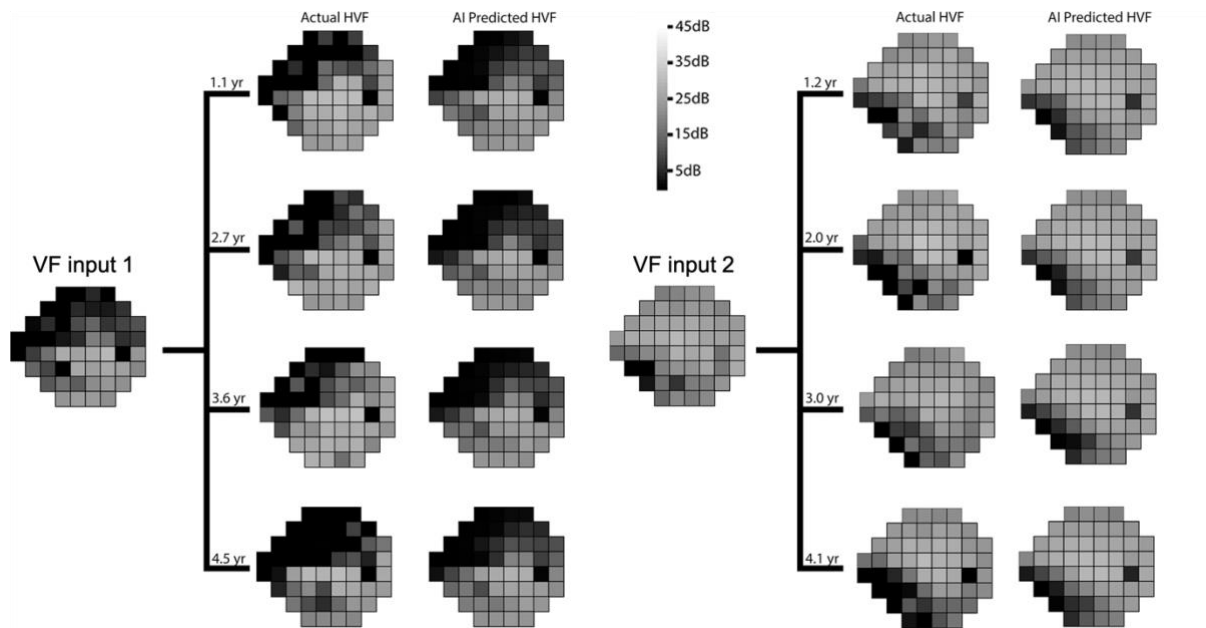


Figure 17. The actual visual field and the AI predicted visual field. The point-wise mean absolute errors for the VF input 1 was 3.8, 3.8, 5.1, and 4.0 dB for 1.1, 2.7, 3.6 and 4.5 years, respectively. And the point-wise mean absolute errors for the VF input 2 was 2.3, 2.5, 3.2, and 3.2 dB for 1.2, 2.0, 3.0 and 4.1 years, respectively. Adapted with permission from Wen et al. Copyright © 2019 Wen et al.

AI systems were also trained to predict glaucoma progression based on structural change assessment. Christopher et al developed a ML system and applied it to OCT images(Christopher et al. 2018). The system significantly detected the glaucomatous structural change and could predict the glaucoma progression by analysing circumpapillary retinal nerve fiber layer (cpRNFL) thickness (AUC 0.74)(Christopher et al. 2018). A CNN-aided algorithm was developed to automatically measure DARC counts, a novel technology to visualize the dead retinal ganglion cells. The CNN system overcame several limitations of manual assessment such as intra- and inter-operator variability. Most importantly, the study showed the system had a potential to predict OCT structural progression of glaucoma(Normando et al. 2020), using a cellular activity measurement.

All things considered, AI has a great potential to enhance glaucoma assessment and monitoring with a reasonable efficiency and accuracy. However, it still has some limitations. For example, huge numbers of images are required to train the AI and the quality of images greatly affects the accuracy of the results. It is challenging and expensive to obtain a vast number of high-quality images to serve as a training set (Devalla et al. 2020; Zheng et al. 2019). Moreover, few studies report the positive predictive value as a measure of accuracy of the AI algorithm. In comparison, the indices that are commonly used to describe the accuracy of AI such as AUC, sensitivity and specificity are subjective, do not really provide the evidence that the probability that subjects with a positive screening test truly have the disease and cannot be directly compared with different studies. Therefore, there is insufficient evidence to summarise the diagnostic performance of an AI model only based on these indices. Further studies are required prior to employing these techniques on a large scale in glaucoma management.

Table 5. Summary of AI studies in glaucoma

Data type	Assessment	Sensitivity	Selectivity	PPV& NPV	Comments	Reference
VF	Diagnostic	-	-	-	Average precision: 87.4±9.5%	Kucur et al. 2018
VF	Diagnostic	93.2%	82.6%	-	Accuracy: 87.60%	Li et al. 2018a
Fundus photography	Diagnostic	98.00%	98.30%	PPV: 98.79%	Accuracy: 98.13%	Raghavendra et al. 2018
Fundus photography	Diagnostic	98.5%	93.3%	PPV: 92.1% NPV: 98.8%	AUC: 0.98	Benzebouchi et al. 2018
RNFL OCT image	Diagnostic	81.1%	77.9%	PPV: 78.6% NPV: 80.5%	Accuracy: 79.5%	Li et al. 2021
Circumpapillary OCT image	Diagnostic	85.1%	96.88%	PPV: 94.44% NPV: 91.18%	Accuracy: 92.3% AUC: 0.9594	García et al. 2020
ONH + VF	Diagnostic	90%	84%	-	Accuracy: 88%	Brigatti et al. 1996
RNFL + VF	Diagnostic	98.3%	97.5%	-	Accuracy: 98% AUC: 0.979	Kim et al. 2017b
VF	Progression	-	-	-	Forecasted VF loss up to 5 years	Wen et al. 2018
RNFL	Progression	-	-	-	AUC: 0.74	Christopher et al. 2018
DARC	Progression	85.7%	91.7%	-	Accuracy: 89.0%	Normando et al. 2020

4. Conclusion

Glaucoma is regarded as a significant public health challenge worldwide(Allison et al. 2020). It significantly impacts the quality of life and has substantial economic effects on both patients and society(Dirani et al. 2011; Quaranta et al. 2016). Early diagnosis of glaucoma therefore is urgently needed. This review summarised both the current clinical tests and emerging technologies to measure the disease activity in glaucoma include IOP test, VF test and OCT(Phu et al. 2020). However, they are suboptimal in some cases. Moreover, sophisticated equipment and well-trained operators are necessary to perform these examinations, making these tests less accessible(Nduaguba and Lee 2006). On the other hand, a study indicated the cost of the conventional glaucoma detection methods (include optic disk tomography, nerve fiber analysis, and tonometry) reached to 1,435€ per case in Spain(Anton et al. 2017). To meet the need of improving glaucoma detection and monitoring, new technologies in development could be valuable supplements to traditional methods.

As a relatively easily accessed fluid of the ocular system, the tear fluid is considered a good source of molecular biomarkers(Hagan et al. 2016). Development of tear-analysing technologies such as microfluidic paper-based devices and contact lenses significantly improve the sensitivity and accuracy of molecular biomarker detection in tears(Park et al. 2018a; Yetisen et al. 2017). More importantly, compared with traditional clinical tests of glaucoma, these devices are more rapid, inexpensive, and user-friendly, which makes them suitable in clinics and at point-of-care settings(Moreddu et al. 2020). However, the analysis of the results remains challenging. Future work will focus on improving novel approaches for more sensitive and specific detection techniques as well as providing clear guideline for sample addition and data processing to increase the reproducibility of the test.

The DARC assesses a unique marker of glaucoma by directly visualising the apoptosis of retinal ganglion cells. The Phase I clinical trial successfully demonstrated the safety and

tolerability of DARC, and it is now undergoing Phase 2 clinical trials(Yap et al. 2020a). It has already been shown to possess the potential to estimate the neurodegeneration in glaucoma patients faster and more cost-effective. With its implementation of artificial intelligence, it can minimise errors caused by manual assessment. However, DARC is a fairly new and experimental technology, further trials are needed in the future. The development of AI significantly increases its diagnostic ability for glaucoma. AI can potentially be an essential adjunct to glaucoma diagnosis in the future. However, getting a large and high-quality training set with several ophthalmic conditions (such as severity of glaucoma or other diseases) and covers all ages, ethnicities is highly recommended to improve the diagnosis ability of AI. Moreover, clear medical guidelines and agreements are also necessary to make it more acceptable. Therefore, in the future, development of AI technologies and multiple comparisons between AI tools and traditional diagnostic practice are still needed. Clinicians can expect the AI tools are able to help in diagnosis in the future.

These promising methods could produce more reliable results in an easier way reducing the reliance on operator skills and environment leading to better glaucoma diagnosis and monitoring. We hope this review will aid future work on the development of novel strategies to monitor glaucoma.

Declaration of competing interest

The authors declare that they have no known competing financial interests or personal relationships that could have appeared to influence the work reported in this paper.

Acknowledgements

A.K.Y and Y.H. thank the Engineering and Physical Sciences Research Council (EP/T013567/1).

Figure 15 was created with BioRender.com.

References

- Acott, T.S., Kelley, M.J., Keller, K.E., Vranka, J.A., Abu-Hassan, D.W., Li, X., Aga, M., Bradley, J.M., 2014. *J Ocul Pharmacol Ther* 30(2-3), 94-101.
- Adornetto, A., Russo, R., Parisi, V., 2019. *Neural Regen Res* 14(3), 391-394.
- Aggarwal, A., Chhabra, K., Kaur, P., Singh, K., Khosa, I., Bansal, P., 2018. *Oman J Ophthalmol* 11(1), 3-10.
- Ahmad, S.S., 2017. *Saudi J Ophthalmol* 31(1), 38-41.
- Alencar, L.M., Medeiros, F.A., 2011. *Indian J Ophthalmol* 59 Suppl, S53-58.
- Allison, K., Patel, D., Alabi, O., 2020. *Cureus* 12(11), e11686.
- Anton, A., Fallon, M., Cots, F., Sebastian, M.A., Morilla-Grasa, A., Mojal, S., Castells, X., 2017. *Clinical ophthalmology (Auckland, N.Z.)* 11, 337-346.
- Araie, M., Iwase, A., Sugiyama, K., Nakazawa, T., Tomita, G., Hangai, M., Yanagi, Y., Murata, H., Tanihara, H., Burgoyne, C.F., Chauhan, B.C., 2017. *Invest Ophthalmol Vis Sci* 58(10), 4106-4113.
- Arora, R., Bellamy, H., Austin, M., 2014. *Clin Ophthalmol* 8, 605-610.
- Aydin, A., Kocak, I., Aykan, U., Can, G., Sabahyildizi, M., Ersanli, D., 2015. *J Fr Ophtalmol* 38(7), 628-632.
- Aziz, K., Friedman, D.S., 2018. *Eye (Lond)* 32(5), 931-937.
- Bang, S.P., Son, M.J., Kim, H., Lee, Y.H., Jun, J.H., 2020. *Sci Rep* 10(1), 15126.
- Benzebouchi, N.E., Azizi, N., Bouziane, S.E., 2018. *International Journal of Advances in Electronics and Computer Science (ijaecs)*.
- Bevers, C., Blanckaert, G., Van Keer, K., Fils, J.F., Vandewalle, E., Stalmans, I., 2019. *Acta Ophthalmol* 97(4), e499-e505.
- Beykin, G., Goldberg, J.L., 2019. *Curr Ophthalmol Rep* 7(3), 171-176.
- Bhattacharya, S.K., Lee, R.K., Grus, F.H., Seventh, A.P.O.R.I.C.W.G., 2013. *Invest Ophthalmol Vis Sci* 54(1), 121-131.
- Bizrah, M., Dakin, S.C., Guo, L., Rahman, F., Parnell, M., Normando, E., Nizari, S., Davis, B., Younis, A., Cordeiro, M.F., 2014. *BMC Bioinformatics* 15, 169.
- Bussel, II, Wollstein, G., Schuman, J.S., 2014. *Br J Ophthalmol* 98 Suppl 2, ii15-19.
- Camp, A.S., Weinreb, R.N., 2017. *Ophthalmology* 124(12S), S71-S75.
- Casson, R.J., Chidlow, G., Wood, J.P., Crowston, J.G., Goldberg, I., 2012. *Clin Exp Ophthalmol* 40(4), 341-349.
- Castro, G.G., Fitt, A.D., Sweeney, J., 2016. *World Journal of Mechanics* 06(03), 35-51.
- Ceruti, P., Morbio, R., Marraffa, M., Marchini, G., 2009. *Eye* 23(2), 262-269.
- Chauhan, B.C., Burgoyne, C.F., 2013. *Am J Ophthalmol* 156(2), 218-227 e212.
- Chen, L., Deng, H., Cui, H., Fang, J., Zuo, Z., Deng, J., Li, Y., Wang, X., Zhao, L., 2018. *Oncotarget* 9(6), 7204-7218.
- Chen, M., Zhang, L., Xu, J., Chen, X., Gu, Y., Ren, Y., Wang, K., 2019. *BMC Ophthalmol* 19(1), 225.
- Christopher, M., Belghith, A., Weinreb, R.N., Bowd, C., Goldbaum, M.H., Saunders, L.J., Medeiros, F.A., Zangwill, L.M., 2018. *Invest Ophthalmol Vis Sci* 59(7), 2748-2756.

Chua, J., Vania, M., Cheung, C.M., Ang, M., Chee, S.P., Yang, H., Li, J., Wong, T.T., 2012. *Mol Vis* 18, 431-438.

Cordeiro, M.F., Hill, D., Patel, R., Corazza, P., Maddison, J., Younis, S., 2021. *Progress in Retinal and Eye Research*, 100976.

Cordeiro, M.F., Normando, E.M., Cardoso, M.J., Miodragovic, S., Jeylani, S., Davis, B.M., Guo, L., Ourselin, S., A'Hern, R., Bloom, P.A., 2017. *Brain* 140(6), 1757-1767.

Costagliola, C., dell'Omo, R., Agnifili, L., Bartollino, S., Fea, A.M., Uva, M.G., Zeppa, L., Mastropasqua, L., 2020. *Surv Ophthalmol* 65(2), 144-170.

Dammeier, S., Martus, P., Klose, F., Seid, M., Bosch, D., D'Alvise, J., Ziemssen, F., Dimopoulos, S., Ueffing, M., 2018. *Transl Vis Sci Technol* 7(6), 22.

Davis, B.M., Crawley, L., Pahlitzsch, M., Javaid, F., Cordeiro, M.F., 2016. *Acta Neuropathol* 132(6), 807-826.

De Moraes, C.G., Liebmann, J.M., Levin, L.A., 2017. *Prog Retin Eye Res* 56, 107-147.

De Tarso Pierre-Filho, P., Gomes, P.R., Pierre, E.T., Pierre, L.M., 2010. *Eur J Ophthalmol* 20(3), 538-541.

Devalla, S.K., Chin, K.S., Mari, J.M., Tun, T.A., Strouthidis, N.G., Aung, T., Thiery, A.H., Girard, M.J.A., 2018. *Invest Ophthalmol Vis Sci* 59(1), 63-74.

Devalla, S.K., Liang, Z., Pham, T.H., Boote, C., Strouthidis, N.G., Thiery, A.H., Girard, M.J.A., 2020. *British Journal of Ophthalmology* 104(3), 301-311.

Dielemans, I., Vingerling, J.R., Hofman, A., Grobbee, D.E., de Jong, P.T., 1994. *Graefes Arch Clin Exp Ophthalmol* 32(3), 141-144.

Dirani, M., Crowston, J.G., Taylor, P.S., Moore, P.T., Rogers, S., Pezzullo, M.L., Keeffe, J.E., Taylor, H.R., 2011. *Clin Exp Ophthalmol* 39(7), 623-632.

Dong, Z.M., Wollstein, G., Schuman, J.S., 2016. *Invest Ophthalmol Vis Sci* 57(9), OCT556-567.

Eliasy, A., Chen, K.J., Vinciguerra, R., Maklad, O., Vinciguerra, P., Ambrosio, R., Jr., Roberts, C.J., Elsheikh, A., 2018. *Exp Eye Res* 175, 98-102.

ElMallah, M.K., Asrani, S.G., 2008. *Curr Opin Ophthalmol* 19(2), 122-126.

Enders, P., Schaub, F., Adler, W., Hermann, M.M., Dietlein, T.S., Cursiefen, C., Heindl, L.M., Medscape, 2018. *Eye (Lond)* 32(2), 314-323.

Esporcatte, L.P.G., Salomao, M.Q., Lopes, B.T., Vinciguerra, P., Vinciguerra, R., Roberts, C., Elsheikh, A., Dawson, D.G., Ambrosio, R., Jr., 2020. *Eye Vis (Lond)* 7, 9.

Fuest, M., Mamas, N., Walter, P., Mazinani, B.E., Roessler, G., Plange, N., 2017. *Curr Eye Res* 42(7), 1007-1012.

Fujimoto, J.G., Pitris, C., Boppart, S.A., Brezinski, M.E., 2000. *Neoplasia* 2(1-2), 9-25.

Fujishiro, T., Matsuura, M., Fujino, Y., Murata, H., Tokumo, K., Nakakura, S., Kiuchi, Y., Asaoka, R., 2020. *J Glaucoma* 29(6), 479-484.

Gao, F., Liu, X., Zhao, Q., Pan, Y., 2017. *Exp Ther Med* 13(5), 1912-1916.

Garas, A., Vargha, P., Hollo, G., 2011. *Eye (Lond)* 25(1), 57-65.

García, G., Amor, R.d., Colomer, A., Naranjo, V., 2020. *Glaucoma Detection From Raw Circumpapillary OCT Images Using Fully Convolutional Neural Networks*. 2020 IEEE International Conference on Image Processing (ICIP), pp. 2526-2530.

Garg, A., De Moraes, C.G., Cioffi, G.A., Girkin, C.A., Medeiros, F.A., Weinreb, R.N., Zangwill, L.M., Liebmann, J.M., 2018. *Am J Ophthalmol* 187, 92-98.

Gelaw, Y., 2012. *BMC Ophthalmology* 12(1), 58.

Ghaffariyeh, A., Honarpisheh, N., Shakiba, Y., Puyan, S., Chamacham, T., Zahedi, F., Zarrineghbal, M., 2009. *Optometry* 80(11), 635-638.

Goldbaum, M.H., Sample, P.A., White, H., Côté, B., Raphaelian, P., Fechtner, R.D., Weinreb, R.N., 1994. *Investigative Ophthalmology & Visual Science* 35(9), 3362-3373.

Goukon, H., Hirasawa, K., Kasahara, M., Matsumura, K., Shoji, N., 2019. *PLoS One* 14(11), e0224711.

Hagan, S., Martin, E., Enriquez-de-Salamanca, A., 2016. *EPMA J* 7, 15.

Harasymowycz, P., Birt, C., Gooi, P., Heckler, L., Hutnik, C., Jinapriya, D., Shuba, L., Yan, D., Day, R., 2016. *J Ophthalmol* 2016, 6509809.

Heijl, A., Patella, V.M., Chong, L.X., Iwase, A., Leung, C.K., Tuulonen, A., Lee, G.C., Callan, T., Bengtsson, B., 2019. *Am J Ophthalmol* 198, 154-165.

Hood, D.C., Raza, A.S., de Moraes, C.G., Liebmann, J.M., Ritch, R., 2013. *Prog Retin Eye Res* 32, 1-21.

Jampel, H.D., Friedman, D., Quigley, H., Vitale, S., Miller, R., Knezevich, F., Ding, Y., 2009. *Am J Ophthalmol* 147(1), 39-44 e31.

Jayanetti, V., Sandhu, S., Lusthaus, J.A., 2020. *J Exp Pharmacol* 12, 539-548.

Jedzierska, M., Koprowski, R., 2019. *Biomed Eng Online* 18(1), 17.

Katsimpris, J.M., Theoulakis, P.E., Vasilopoulos, K., Skourtis, G., Papadopoulos, G.E., Petropoulos, I.K., 2015. *Klin Monbl Augenheilkd* 232(4), 414-418.

Kaur, P., Khosla, P.K., 2020. Artificial Intelligence Based Glaucoma Detection. In: Verma, O.P., Roy, S., Pandey, S.C., Mittal, M. (Eds.), *Advancement of Machine Intelligence in Interactive Medical Image Analysis*, pp. 283-305. Springer Singapore, Singapore.

Kilavuzoglu, A.E.B., Cosar, C.B., Celebi, A.R., Al Parmak, U.E., 2019. *J Curr Glaucoma Pract* 13(2), 68-73.

Kim, D.W., Seo, J.H., Lim, S.H., 2021. *Eye (Lond)* 35(3), 892-900.

Kim, H.J., Seo, Y.H., Kim, B.H., 2017a. *PLOS ONE* 12(12), e0186738.

Kim, S.J., Cho, K.J., Oh, S., 2017b. *PloS one* 12(5), e0177726.

Kimura, T., Matsumoto, C., Nomoto, H., 2019. *Clin Ophthalmol* 13, 501-513.

Koczula, Katarzyna M., Gallotta, A., 2016. *Essays in Biochemistry* 60(1), 111-120.

Kuang, T.M., Zhang, C., Zangwill, L.M., Weinreb, R.N., Medeiros, F.A., 2015. *Ophthalmology* 122(10), 2002-2009.

Kucur, S.S., Hollo, G., Sznitman, R., 2018. *PLoS One* 13(11), e0206081.

Kumagai, T., Shoji, T., Yoshikawa, Y., Mine, I., Kanno, J., Ishii, H., Saito, A., Ishikawa, S., Kimura, I., Shinoda, K., 2020. *Br J Ophthalmol* 104(11), 1258-1534.

Kuryshva, N.I., Lepeshkina, L.V., 2021. *J Glaucoma*.

Lam, T., Devadhasan, J.P., Howse, R., Kim, J., 2017. *Scientific Reports* 7(1), 1188.

Lazcano-Gomez, G., Ramos-Cadena, M.L.A., Torres-Tamayo, M., Hernandez de Oteyza, A., Turati-Acosta, M., Jimenez-Román, J., 2016. *Medicine (Baltimore)* 95(47), e5341.

Leaney, J.C., Nguyen, V., Miranda, E., Barnett, Y., Ahmad, K., Wong, S., Lawlor, M., 2020. *Am J Ophthalmol* 218, 164-172.

Lee, P.P., Walt, J.G., Doyle, J.J., Kotak, S.V., Evans, S.J., Budenz, D.L., Chen, P.P., Coleman, A.L., Feldman, R.M., Jampel, H.D., Katz, L.J., Mills, R.P., Myers, J.S., Noecker, R.J., Piltz-Seymour, J.R., Ritch, R.R., Schacknow, P.N., Serle, J.B., Trick, G.L., 2006. *Archives of Ophthalmology* 124(1), 12-19.

Lee, S.Y., Lee, E.K., Park, K.H., Kim, D.M., Jeoung, J.W., 2016a. *PLoS One* 11(10), e0164866.

Lee, T.H., Heo, H., Park, S.W., 2016b. *Chonnam Med J* 52(3), 194-200.

Leung, C.K., 2014. *Curr Opin Ophthalmol* 25(2), 104-111.

Li, F., Wang, Z., Qu, G., Song, D., Yuan, Y., Xu, Y., Gao, K., Luo, G., Xiao, Z., Lam, D.S.C., Zhong, H., Qiao, Y., Zhang, X., 2018a. *BMC Medical Imaging* 18(1).

Li, L., Zhu, H., Zhang, Z., Zhao, L., Xu, L., Jonas, R.A., Garway-Heath, D.F., Jonas, J.B., Wang, Y.X., 2021. *JMIR Med Inform* 9(5), e22664-e22664.

Li, Z., He, Y., Keel, S., Meng, W., Chang, R.T., He, M., 2018b. *Ophthalmology* 125(8), 1199-1206.

Liu, H., Li, L., Wormstone, I.M., Qiao, C., Zhang, C., Liu, P., Li, S., Wang, H., Mou, D., Pang, R., Yang, D., Jiang, L., Chen, Y., Hu, M., Xu, Y., Kang, H., Ji, X., Chang, R., Tham, C., Cheung, C., Ting, D.S.W., Wong, T.Y., Wang, Z., Weinreb, R.N., Xu, M., Wang, N., 2019. *JAMA Ophthalmol* 137(12), 1353-1360.

Liu, J., De Francesco, T., Schlenker, M., Ahmed, II, 2020. *Clin Ophthalmol* 14, 4031-4045.

Liu, W., Li, H., Lu, D., Liang, J., Xing, X., Liu, A., Zhao, S., Li, X., Ji, J., 2010. *Mol Vis* 16, 2342-2346.

Matsumoto, C., Yamao, S., Nomoto, H., Takada, S., Okuyama, S., Kimura, S., Yamanaka, K., Aihara, M., Shimomura, Y., 2016. *PLoS One* 11(8), e0161974.

Mayro, E.L., Wang, M., Elze, T., Pasquale, L.R., 2019. *Eye* 34(1), 1-11.

McCann, P., Hogg, R.E., Wright, D.M., McGuinness, B., Young, I.S., Kee, F., Azuara-Blanco, A., 2020. *Eye (Lond)* 34(3), 584-590.

McNally, S., O'Brien, C.J., 2014. *J Glaucoma* 23(8 Suppl 1), S51-54.

Messmer, E.M., von Lindenfels, V., Garbe, A., Kampik, A., 2016. *Ophthalmology* 123(11), 2300-2308.

Miocevic, O., Cole, C.R., Laughlin, M.J., Buck, R.L., Slowey, P.D., Shirtcliff, E.A., 2017. *Front Public Health* 5, 133.

Miri, M.S., Abràmoff, M.D., Kwon, Y.H., Sonka, M., Garvin, M.K., 2017. *Medical Image Analysis* 39, 206-217.

Miri, M.S., Abràmoff, M.D., Lee, K., Niemeijer, M., Wang, J.K., Kwon, Y.H., Garvin, M.K., 2015. *IEEE Trans Med Imaging* 34(9), 1854-1866.

Moreddu, R., Vigolo, D., Yetisen, A.K., 2019. *Adv Healthc Mater* 8(15), e1900368.

Moreddu, R., Wolffsohn, J.S., Vigolo, D., Yetisen, A.K., 2020. *Sensors and Actuators B: Chemical* 317, 128183.

Moshirfar, M., Pierson, K., Hanamaikai, K., Santiago-Caban, L., Muthappan, V., Passi, S.F., 2014. *Clin Ophthalmol* 8, 1419-1433.

Muramatsu, C., Hayashi, Y., Sawada, A., Hatanaka, Y., Hara, T., Yamamoto, T., Fujita, H., 2010. *J Biomed Opt* 15(1), 016021.

Mursch-Edlmayr, A.S., Ng, W.S., Diniz-Filho, A., Sousa, D.C., Arnold, L., Schlenker, M.B., Duenas-Angeles, K., Keane, P.A., Crowston, J.G., Jayaram, H., 2020. *Transl Vis Sci Technol* 9(2), 55.

Muth, D.R., Hirneiss, C.W., 2015. *Invest Ophthalmol Vis Sci* 56(5), 3320-3328.

Mwanza, J.C., Budenz, D.L., 2016. *Curr Opin Ophthalmol* 27(2), 102-110.

Mwanza, J.C., Oakley, J.D., Budenz, D.L., Anderson, D.R., Cirrus Optical Coherence Tomography Normative Database Study, G., 2011. *Ophthalmology* 118(2), 241-248 e241.

Mysona, B.A., Zhao, J., Bollinger, K.E., 2017. *Expert Rev Ophthalmol* 12(1), 69-81.

Nduaguba, C., Lee, R.K., 2006. *Current Opinion in Ophthalmology* 17(2), 142-152.

Normando, E.M., Turner, L.A., Cordeiro, M.F., 2013. *Cell Tissue Res* 353(2), 279-285.

Normando, E.M., Yap, T.E., Maddison, J., Miodragovic, S., Bonetti, P., Almonte, M., Mohammad, N.G., Ameen, S., Crawley, L., Ahmed, F., Bloom, P.A., Cordeiro, M.F., 2020. *Expert Rev Mol Diagn* 20(7), 737-748.

Nouri-Mahdavi, K., 2014. *Can J Ophthalmol* 49(6), 497-505.

Nuyen, B., Mansouri, K., 2015. *Asia Pac J Ophthalmol (Phila)* 4(2), 66-75.

Oddone, F., Roberti, G., Micera, A., Busanello, A., Bonini, S., Quaranta, L., Agnifili, L., Manni, G., 2017. *PLoS One* 12(1), e0168565.

Okafor, K.C., Brandt, J.D., 2015. *Curr Opin Ophthalmol* 26(2), 103-109.

Olyntho Junior, M.A.C., Augusto, L.B., Gracitelli, C.P.B., Tatham, A.J., 2020. *Vision (Basel)* 4(4).

Pan, C.W., Ke, C., Chen, Q., Tao, Y.J., Zha, X., Zhang, Y.P., Zhong, H., 2020. *BMC Ophthalmol* 20(1), 183.

Papastergiou, G.I., Kozobolis, V., Siganos, D.S., 2008. *J Glaucoma* 17(6), 484-488.

Park, J., Kim, J., Kim, S.Y., Cheong, W.H., Jang, J., Park, Y.G., Na, K., Kim, Y.T., Heo, J.H., Lee, C.Y., Lee, J.H., Bien, F., Park, J.U., 2018a. *Sci Adv* 4(1), eaap9841.

Park, K., Kim, J., Lee, J., 2018b. *J Glaucoma* 27(9), 750-760.

Park, S.C., Kung, Y., Su, D., Simonson, J.L., Furlanetto, R.L., Liebmann, J.M., Ritch, R., 2013. *Ophthalmology* 120(8), 1546-1550.

Pekel, G., Acer, S., Yagci, R., Kaya, H., Ozbakis, F., Bahar, A., Cetin, E.N., 2015. *Kaohsiung J Med Sci* 31(8), 420-425.

Phu, J., Khuu, S.K., Agar, A., Domadiou, I., Ng, A., Kalloniatis, M., 2020. *Ophthalmology Glaucoma* 3(4), 274-287.

Phu, J., Khuu, S.K., Yapp, M., Assaad, N., Hennessy, M.P., Kalloniatis, M., 2017. *Clin Exp Optom* 100(4), 313-332.

Pieragostino, D., Agnifili, L., Fasanella, V., D'Aguanno, S., Mastropasqua, R., Di Ilio, C., Sacchetta, P., Urbani, A., Del Boccio, P., 2013. *Mol Biosyst* 9(6), 1108-1116.

Pilat, A.V., Shah, S., Sheth, V., Purohit, R., Proudlock, F.A., Abbott, J., Gottlob, I., 2019. *BMJ Open Ophthalmol* 4(1), e000194.

Prabhakar, B., Singh, R.K., Yadav, K.S., 2021. *Comput Med Imaging Graph* 87, 101818.

Quaranta, L., Riva, I., Gerardi, C., Oddone, F., Floriani, I., Konstas, A.G., 2016. *Adv Ther* 33(6), 959-981.

Raghavendra, U., Fujita, H., Bhandary, S.V., Gudigar, A., Tan, J.H., Acharya, U.R., 2018. *Information Sciences* 441, 41-49.

Ramm, L., Herber, R., Spoerl, E., Raiskup, F., Pillunat, L.E., Terai, N., 2019. *J Ophthalmol* 2019, 3879651.

Ran, A.R., Cheung, C.Y., Wang, X., Chen, H., Luo, L.-y., Chan, P.P., Wong, M.O.M., Chang, R.T., Mannil, S.S., Young, A.L., Yung, H.-w., Pang, C.P., Heng, P.-A., Tham, C.C., 2019. *The Lancet Digital Health* 1(4), e172-e182.

Rieck, J., 2013. *Invest Ophthalmol Vis Sci* 54(3), 2393-2409.

Roberti, G., Manni, G., Riva, I., Hollo, G., Quaranta, L., Agnifili, L., Figus, M., Giammaria, S., Rastelli, D., Oddone, F., 2017. *PLoS One* 12(10), e0186793.

Roedl, J.B., Bleich, S., Schlotzer-Schrehardt, U., von Ahsen, N., Kornhuber, J., Naumann, G.O., Kruse, F.E., Junemann, A.G., 2008. *Ophthalmic Res* 40(5), 249-256.

Rowe, F.J., Czanner, G., Somerville, T., Sood, I., Sood, D., 2021. *Curr Eye Res* 46(1), 83-95.

Rowe, F.J., Rowlands, A., 2014. *BioMed Research International* 2014, 214829.

Sahay, P., Rao, A., Padhy, D., Sarangi, S., Das, G., Reddy, M.M., Modak, R., 2017. *Invest Ophthalmol Vis Sci* 58(6), BIO106-BIO113.

Salazar, H., Misra, V., Swaminathan, S.S., 2021. *Curr Opin Ophthalmol* 32(2), 105-117.

Saleh, T.A., McDermott, B., Bates, A.K., Ewings, P., 2006. *Eye (Lond)* 20(8), 913-915.

Sambursky, R., Davitt, W.F., 3rd, Friedberg, M., Tauber, S., 2014. *Cornea* 33(8), 812-818.

Sambursky, R., Davitt, W.F., 3rd, Latkany, R., Tauber, S., Starr, C., Friedberg, M., Dirks, M.S., McDonald, M., 2013. *JAMA Ophthalmol* 131(1), 24-28.

Sayah, D.N., Mazzaferri, J., Descovich, D., Costantino, S., Lesk, M.R., 2020. *Invest Ophthalmol Vis Sci* 61(13), 11.

Schuster, A.K., Erb, C., Hoffmann, E.M., Dietlein, T., Pfeiffer, N., 2020. *Dtsch Arztebl Int* 117(13), 225-234.

Sedaghat, M.R., Momeni-Moghaddam, H., Yekta, A., Elsheikh, A., Khabazkhoob, M., Ambrosio, R., Jr., Maddah, N., Danesh, Z., 2019. *Clin Optom (Auckl)* 11, 127-133.

Shpak, A.A., Guekht, A.B., Druzhkova, T.A., Kozlova, K.I., Gulyaeva, N.V., 2018. *Curr Eye Res* 43(2), 224-231.

Singh, D., Srivastava, S.K., Chaudhuri, T.K., Upadhyay, G., 2015. *Front Mol Biosci* 2, 19.

Sng, C.C., Ang, M., Barton, K., 2017. *Curr Opin Ophthalmol* 28(2), 120-126.

Sonobe, H., Ogawa, Y., Yamada, K., Shimizu, E., Uchino, Y., Kamoi, M., Saijo, Y., Yamane, M., Citterio, D., Suzuki, K., Tsubota, K., 2019. *The Ocular Surface* 17(1), 160-166.

Stamper, R.L., 2011. *Optom Vis Sci* 88(1), E16-28.

Subramaniam, A.G., Allen, P., Toh, T., 2020. *Ophthalmic Res.*

Sugisaki, K., Asaoka, R., Inoue, T., Yoshikawa, K., Kanamori, A., Yamazaki, Y., Ishikawa, S., Nemoto, H., Iwase, A., Araie, M., 2020. *British Journal of Ophthalmology* 104(5), 642-647.

Szatmáry, G., Biousse, V., Newman, N.J., 2002. *Archives of Ophthalmology* 120(9), 1162-1173.

Takada, N., Omodaka, K., Kikawa, T., Takagi, A., Matsumoto, A., Yokoyama, Y., Shiga, Y., Maruyama, K., Takahashi, H., Akiba, M., Nakazawa, T., 2016. *PLoS One* 11(8), e0160226.

Tan, S., Yu, M., Baig, N., Hansapinyo, L., Tham, C.C., 2017. *Sci Rep* 7, 42067.

Tatham, A.J., Medeiros, F.A., 2017. *Ophthalmology* 124(12S), S57-S65.

Tezel, G., Wax, M.B., 2004. *Curr Opin Ophthalmol* 15(2), 80-84.

Tham, Y.C., Li, X., Wong, T.Y., Quigley, H.A., Aung, T., Cheng, C.Y., 2014. *Ophthalmology* 121(11), 2081-2090.

Thompson, A.C., Jammal, A.A., Medeiros, F.A., 2019. *Am J Ophthalmol* 201, 9-18.

Tomairek, R.H., Aboud, S.A., Hassan, M., Mohamed, A.H., 2020. *Eur J Ophthalmol* 30(4), 706-713.

Tomlinson, A., Blades, K.J., Pearce, E.I., 2001. *Optom Vis Sci* 78(3), 142-146.

Traverso, C.E., Walt, J.G., Kelly, S.P., Hommer, A.H., Bron, A.M., Denis, P., Nordmann, J.-P., Renard, J.-P., Bayer, A., Grehn, F., Pfeiffer, N., Cedrone, C., Gandolfi, S., Orzalesi, N., Nucci, C., Rossetti, L., Azuara-Blanco, A., Bagnis, A., Hitchings, R., Salmon, J.F., Bricola, G., Buchholz, P.M., Kotak, S.V., Katz, L.M., Siegartel, L.R., Doyle, J.J., 2005. *British Journal of Ophthalmology* 89(10), 1245-1249.

Uzlu, D., Akyol, N., Turk, A., Oruc, Y., 2020. *Int Ophthalmol* 40(8), 1999-2005.

Varma, R., Lee, P.P., Goldberg, I., Kotak, S., 2011. *Am J Ophthalmol* 152(4), 515-522.

Vazquez, L.E., Bye, A., Aref, A.A., 2021. *Curr Opin Ophthalmol* 32(2), 98-104.

Verticchio Vercellin, A.C., Jassim, F., Poon, L.Y., Tsikata, E., Braaf, B., Shah, S., Ben-David, G., Shieh, E., Lee, R., Simavli, H., Que, C.J., Papadogeorgou, G., Guo, R., Vakoc, B.J., Bouma, B.E., de Boer, J.F., Chen, T.C., 2018. *Invest Ophthalmol Vis Sci* 59(12), 4998-5010.

Vinciguerra, R., Rehman, S., Vallabh, N.A., Batterbury, M., Czanner, G., Choudhary, A., Cheeseman, R., Elsheikh, A., Willoughby, C.E., 2020. *Br J Ophthalmol* 104(1), 121-126.

Wang, M., Shen, L.Q., Pasquale, L.R., Petrakos, P., Formica, S., Boland, M.V., Wellik, S.R., De Moraes, C.G., Myers, J.S., Saeedi, O., Wang, H., Baniyadi, N., Li, D., Tichelaar, J., Bex, P.J., Elze, T., 2019. *Invest Ophthalmol Vis Sci* 60(1), 365-375.

Wang, X., McAlinden, C., Zhang, H., Yan, J., Wang, D., Wei, W., Mi, S., 2021. *Sci Rep* 11(1), 3041.

Wang, Y., Henson, D.B., 2013. *Invest Ophthalmol Vis Sci* 54(1), 756-761.

Weinreb, R.N., Aung, T., Medeiros, F.A., 2014. *JAMA* 311(18), 1901-1911.

Wen, J., Lee, C., Keane, P., Xiao, S., Wu, Y., Rokem, A., Chen, P., Lee, A., 2018. *PLoS ONE* 14.

Wu, H., de Boer, J.F., Chen, T.C., 2012. *Am J Ophthalmol* 153(5), 815-826 e812.

Wu, Y.-c., Feng, J.-w., 2017. *Wireless Personal Communications* 102(2), 1645-1656.

Wu, Z., Medeiros, F.A., 2018. *Curr Opin Ophthalmol* 29(2), 141-146.

Wu, Z., Medeiros, F.A., Weinreb, R.N., Zangwill, L.M., 2018. *Am J Ophthalmol* 196, 10-17.

Yamada, H., Hangai, M., Nakano, N., Takayama, K., Kimura, Y., Miyake, M., Akagi, T., Ikeda, H.O., Noma, H., Yoshimura, N., 2014a. *Am J Ophthalmol* 158(6), 1318-1329 e1313.

Yamada, K., Takaki, S., Komuro, N., Suzuki, K., Citterio, D., 2014b. *Analyst* 139(7), 1637-1643.

Yap, T.E., Donna, P., Almonte, M.T., Cordeiro, M.F., 2018a. *Cells* 7(6).

Yap, T.E., Normando, E.M., Cordeiro, M.F., 2018b. *Expert Review of Ophthalmology* 13(2), 113-127.

Yap, T.E., Shamsheer, E., Guo, L., Cordeiro, M.F., 2020a. *Ophthalmic Res* 63(1), 1-7.

Yap, T.E., Szymanska, M., Cordeiro, M.F., 2020b. *Advances in Retinal Imaging: Real-Time Imaging of Single Neuronal Cell Apoptosis (DARC)*. In: Grzybowski, A., Barboni, P. (Eds.), *OCT and Imaging in Central Nervous System Diseases: The Eye as a Window to the Brain*, pp. 123-138. Springer International Publishing, Cham.

Yaqub, M., 2012. *Community Eye Health* 25(79-80), 1-8.

Yetisen, A.K., Akram, M.S., Lowe, C.R., 2013. *Lab Chip* 13(12), 2210-2251.

Yetisen, A.K., Jiang, N., Castaneda Gonzalez, C.M., Erenoglu, Z.I., Dong, J., Dong, X., Stosser, S., Brischwein, M., Butt, H., Cordeiro, M.F., Jakobi, M., Hayden, O., Koch, A.W., 2020. *Adv Mater* 32(6), e1906762.

Yetisen, A.K., Jiang, N., Tamayol, A., Ruiz-Esparza, G.U., Zhang, Y.S., Medina-Pando, S., Gupta, A., Wolffsohn, J.S., Butt, H., Khademhosseini, A., Yun, S.H., 2017. *Lab Chip* 17(6), 1137-1148.

Yildiz, A., Yasar, T., 2018. *Med Glas (Zenica)* 15(2), 152-157.

Yousefi, S., Kiwaki, T., Zheng, Y., Sugiura, H., Asaoka, R., Murata, H., Lemij, H., Yamanishi, K., 2018. *American Journal of Ophthalmology* 193, 71-79.

Zakrzewska, A., Wiącek, M.P., Machalińska, A., 2019. *Int J Ophthalmol* 12(12), 1853-1858.

Zha, Y., Huang, W., Zhuang, J., Cai, J., 2019. *BMC Ophthalmol* 19(1), 36.

Zheng, C., Johnson, T.V., Garg, A., Boland, M.V., 2019. *Curr Opin Ophthalmol* 30(2), 97-103.